R-99-62

Application of the multirate diffusion approach in tracer test studies at Äspö HRL

Roy Haggerty
Department of Geosciences,
Oregon State University, USA

November 1999

Svensk Kärnbränslehantering AB
Swedish Nuclear Fuel
and Waste Management Co
Box 5864
SE-102 40 Stockholm Sweden
Tel 08-459 84 00
+46 8 459 84 00
Fax 08-661 57 19
+46 8 661 57 19

ISSN 1402-3091
SKB Rapport R-99-62

Application of the multirate diffusion approach in tracer test studies at Äspö HRL

Final report

Roy Haggerty
Department of Geosciences,
Oregon State University, USA

November 1999

Keywords: multirate diffusion, anomalous diffusion, heterogeneous diffusion, long-term diffusion experiment, breakthrough curve slope, power-law, fractal, characteristic time-scale.

Summary

This report summarizes an investigation into heterogeneous diffusivity and associated parameters within granitic rocks at the Äspö Hard Rock Laboratory (HRL). "Anomalous diffusion" /Havlin and Ben-Avraham, 1987; Bouchaud and Georges, 1990/ refers to diffusion that is non-Fickian, and for our purposes, sub-diffusive. Such sub-diffusive behavior typically results from strong geometric disorder within the pore structure of the rock. "Multirate diffusion" /Haggerty and Gorelick, 1995, 1998/ is a more general concept that may include anomalous diffusion; in general multirate diffusion refers to multiple diffusion rate coefficients (i.e., a distribution of D_d/a^2) present within a volume of rock that is small with respect to advection distances. A distribution of D_d/a^2 results from variability in any of (1) matrix block size; (2) pore geometry (tortuosity, cross-sectional area, and connectivity); and (3) sorption capacity and strength.

Our tasks for this investigation were: (1) to assess the potential for either anomalous or multirate diffusion within Äspö rocks; (2) to evaluate existing data relating to anomalous and multirate diffusion within Äspö rocks; (3) to perform scoping calculations in support of a Long Term Diffusion Experiment (LTDE) design; and (4) to begin developing a mathematical and computer model for solute advection in the presence of anomalous matrix diffusion. In addition to carrying out these tasks, we also report on (5) the late-time behavior of breakthrough curves. Key points follow.

First, in regard to the potential for anomalous and multirate diffusion and analyses of existing data, we find that (1) in a literature review of 100 column experiments (Section 3.1) in various types of rock and sediment, rate coefficients decrease with experimental observation time. This is precisely what would be expected of both multirate and anomalous diffusion. (2) Three sets of through-diffusion experiments in Fenno-Scandian granitic rock found decreasing effective diffusivity, D_e, with sample length, while one set did not. Decreasing D_e with sample length is evidence for anomalous diffusion. (3) Based on diffusivity and sorption data, and speculation on matrix block size variability, the total variability of D_d/a^2 may reasonably be expected to exceed 4 orders of magnitude. (4) Analyses of two-well tracer data completed to date are ambiguous with respect to multirate diffusion. Analyses of TRUE data are currently underway and may support multirate diffusion.

Second, in regard to the potential consequences of multirate and anomalous diffusion on nuclear waste disposal, we found the following key points (true only if either anomalous or multirate diffusion occur). (1) No single value of diffusivity can represent the diffusion process at all time- or length-scales if diffusion is truly anomalous, while a single value of diffusivity will represent diffusion adequately for some cases of multirate diffusion. (2) For both multirate and anomalous diffusion the diffusivity may decrease with time- and length-scale of measurement, making the parameter value dependent upon the experimental design. (3) A transport model using a single diffusion rate coefficient and that assumes the total matrix porosity is accessible by diffusion will over-estimate the late-time retardation of the solute plume. Performance Assessment transport calculations would therefore be non-conservative.

Third, with respect to our scoping calculations for the LTDE, we make the following points. (1) Maximum information regarding heterogeneity in diffusivity will be obtained with monitoring back-diffusion data from either an injected (long-term) or natural tracer. Both must be measured over several decades of concentration and time. (2) Care must be taken not to misinterpret heterogeneity in diffusivity as a single diffusivity but with higher value. Several concentration histories in the scoping calculations indicate that a model allowing only a single diffusivity may yield an estimate of diffusivity that is too large. (3) The radial nature of the geometry used in the scoping calculations interes to some extent with current methods of identifying multirate diffusion.

Fourth, in regard to incorporation of anomalous matrix diffusion into a solute transport model, we report the following. (1) We are in the process of developing a renormalization methodology that allows diffusion on a fractal matrix while allowing advection and dispersion. Preliminary results indicate that this is feasible and extremely efficient. (2) Resulting late-time breakthrough curves behave as a power-law.

Fifth, in regard to the late-time behavior of breakthrough curves, we investigated the late-time behavior of tracer test breakthrough curves with rate-limited mass transfer and found that the late-time concentration is given by the simple expression:

$$c = t_{ad}\left(c_0 g - m_0 \frac{\partial g}{\partial t}\right), \quad t >> t_{ad} \; and \; t_\alpha >> t_{ad}$$

where t_{ad} is the advection time, c_0 is the initial concentration in the medium, m_0 is the 0^{th} moment of the injection pulse; and $t_{\cdot}$ is the mean residence time in the immobile zone. The function g is proportional to the residence time distribution in the immobile zone; g is well-known for many geometries and we give it for several distributed (multirate) models of mass transfer. Using this expression we examine the behavior of late-time concentration for a number of mass transfer models. The following are some of the key points. (1) If rate-limited mass transfer causes late-time concentration to go as t^{-k}, then the underlying distribution of rate coefficients must be α^{k-3} as $\alpha \rightarrow 0$. This is true for both distributions of first-order and diffusion rate coefficients. (2) Breakthrough curves with $k < 3$ persisting to the end of the experiment indicate a mean matrix residence time longer than the experiment and possibly infinite, and indicate an effective rate coefficient that is either undefined or changes as a function of observation time. (3) Breakthrough curves with $k < 3$ persisting to the end of the experiment indicate that it is not possible to estimate a characteristic mass transfer time based on the experimental data (i.e., that the characteristic mass transfer time-scale is at least as long as the experiment).

Recommendations:

Based on the findings of our investigation, we make the following recommendations.

1. Current efforts with the LTDE give high priority to investigation of heterogeneity in diffusivity at Äspö. This should include an attempt to optimize the experiment in terms of its capability to extract information about the distribution of diffusion rate coefficients within the rock. It should also include modeling the data with a code capable of multirate diffusion. The latter is needed because an a priori assumption of a single (homogeneous) diffusivity may result in an overestimation of the diffusivity.

2. A theoretical/mathematical study be undertaken to determine the consequences on Performance Assessment of both (a) multirate diffusion with various distributions of rate coefficients, including lognormal with large α and power-law; and (b) anomalous diffusion with sub-diffusive behavior.

3. Laboratory work should be undertaken to examine multirate and anomalous diffusion within Äspö rocks. At a minimum this would include (a) a detailed examination of the pore structure of the rock, with attention to fractal geometry and fractal dimension; and (2) laboratory experiments optimized to identify either or both multirate and anomalous diffusion.

Table of contents

1 Introduction

The Äspö Hard Rock Laboratory (HRL) has been constructed as part of the preparations for a deep geologic repository for spent nuclear fuel in Sweden. One of the defined stage goals of Äspö HRL is to test methods for description of the barrier function of the host rock. The ongoing Tracer Retention Understanding Experiment (TRUE) is aimed at developing an understanding of radionuclide migration and retention in fractured rock and to evaluate to what extent concepts used in models are based on realistic descriptions of the rock. One of the most important retention processes from a Performance Assessment (PA) perspective is matrix diffusion, i.e., diffusion into the stagnant water of the low permeability rock matrix surrounding the more conductive fractures. However, sorption on fracture surfaces (and possibly gauge material) may be a more dominant retention process than matrix diffusion for the experimental conditions of TRUE. A complimentary field experiment, the Long Term Diffusion Experiment (LTDE) is thus planned to specifically address diffusion issues in low permeability rock. The combined information from TRUE (advective transport in fractures combined with general retention processes) and LTDE (diffusive transport in low permeability rock) is believed to provide relevant knowledge for formulating realistic radionuclide transport models for performance assessment of the barrier function of the host rock.

A number of studies have shown that the diffusivities of crystalline geologic media are heterogeneous /e.g., Valkiainen, 1992; Ohlsson and Neretnieks, 1995, 1997; Xu and Worman, 1997; and others/. This heterogeneity appears over a wide range of scales: for example, a single rock from one borehole may have a highly variable diffusivity over distances of mm to cm /e.g., Ittner et al, 1990; Tsukamoto and Ohe, 1993; Johansson et al, 1998; and others/. Pore-scale and micro-pore-scale variability certainly extend the variability in diffusivities to scales approaching molecular /e.g., Lovera et al, 1989, 1993; Hollewand and Gladden, 1995; Werth et al, 1997/, while variability in rock-type, structure, and geologic history extend this variability to much larger distances /e.g., Wadden and Katsube, 1982/.

Heterogeneity in diffusivities is due to a number of factors. In addition to those already mentioned, diffusivities vary due to (1) the types of minerals and their spatial distributions; (2) geometry, chemistry, and mineralogy of coatings on the surfaces of fractures or grains; (3) the volume, size, geometry, connectivity and distribution of all pore space in the rock /after Haggerty and Gorelick, 1998/. In addition to these sources of heterogeneity, the size of matrix blocks in a fractured rock may vary considerably, thus modifying the time-scales for diffusion into and out of the rock.

Diffusive heterogeneity leads to a number of difficulties if a model that assumes a homogeneous effective diffusivity (or matrix block size) is used to describe field-scale transport of radionuclides. First, it is unclear what effective diffusivity should be used. As we know from the literature on effective hydraulic conductivities, it can be an extremely challenging matter to determine an effective parameter for a heterogeneous medium e.g., Gelhar, 1993/. Second, the diffusivity may become a function of the observation time-scale or spatial-scale. A number of experimental results now suggest that diffusivities (or diffusion rate coefficients, which are diffusion rate coefficients divided by a length-scale squared) may be dependent upon the time-scale or spatial-scale of observation /Valkiainen et al, 1996; Haggerty and Harvey, 1997; Johansson et

al, 1997; Haggerty and Gorelick, 1998/. Third, if diffusivities measured at the laboratory time- and spatial-scale are different than those that would be effective at the PA-scale, then a conventional model assuming homogeneous diffusivities could over-predict transport time for radionuclides or under-predict mass release.

Four main tasks were proposed for this project: five tasks were completed. These tasks are as follows:

1. Assessment of potential for anomalous or multirate diffusion (Section 3);

2. Evaluation of existing data (Section 3);

3. Scoping calculations for LTDE (Section 4);

4. Development of an advection-anomalous diffusion model (Section 5); and

5. Examination of information available on matrix diffusion from the late-time slope of a breakthrough curve (Section 6).

Tasks 1 through 4 were proposed as part of the project. Tasks 1 and 2 were completed more-or-less as envisioned in the Testplan. Task 3 was modified to concentrate on scoping calculations that were to be used in assisting a Testplan development for the LTDE /e.g., Byegård et al, 1999/. Although the design for the LTDE is being modified from that which we conducted our scoping calculations on, we hope that the calculations we have completed are of value to the LTDE project.

Due to the complex nature of Task 4, it was expected that this would be only started during this project. As it stands, we have developed a theoretical foundation for advection with anomalous matrix diffusion (something we were uncertain if we would be able to do), but we have not yet fully investigated the implications and consequences of this.

Task 5 was added at our discretion. Examination of the late-time behavior of breakthrough curves is clearly relevant to tracer tests conducted at Äspö (e.g., TRUE). At the same time, we have been working with a theoretical foundation for extracting matrix diffusion information from the late-time behavior of breakthrough curves. Section 6 lays out this foundation. We hope that this information will be of assistance to the ongoing work at Äspö.

2 Overview of anomalous and multirate diffusion

2.1 Anomalous diffusion

Models that employ diffusive mass transfer between matrix blocks and fractures describe the concentration within the block with Fick's Law and mass conservation. Matrix blocks are typically assumed to be an idealized Euclidian geometry, such as a sphere or slab with a homogeneous diffusivity. In the case of a spherical matrix block (for example), concentration (c_m) is given by the solution of the diffusion equation /Crank, 1975/:

$$\frac{\partial c_m}{\partial t} = \frac{D_a}{r^2}\frac{\partial}{\partial z}\left(r^2\frac{\partial c_m}{\partial r}\right) \text{ , } 0 \le r \le a \qquad (2\text{-}1)$$

where all variables are defined in the Appendix (Section 9).

The primary concern with such a Euclidian formulation is not the assumed spherical shape of the matrix block or the magnitude of the apparent diffusivity, but that the pore-space within the immobile zone is assumed to be both Euclidian and homogeneous (or at least homogenizable). In cases where the matrix is not Euclidian (such as a fractal pore geometry), however, diffusion may not be described by the diffusion equation. Although the apparent diffusivity can be scaled to include tortuosity or the effects of other phenomena such as sorption, constrictivity, or steric hindrance /e.g., Satterfield et al, 1973; Farrell and Reinhard, 1994; Ohlsson and Neretnieks, 1997/, the diffusion process may be mathematically non-Fickian, and therefore Eqn. (2-1) will not apply. Such diffusion has been termed "anomalous" /e.g., Havlin and Ben-Avraham, 1987; Bouchaud and Georges, 1990/.

Recent work, primarily in applied physics and chemical engineering has shown that Eqn. (2-1) does not apply in cases where diffusion takes place in a geometrically complex, or disordered space, such as a fractal /e.g., Havlin and Ben-Avraham, 1987; Sheintuch and Brandon, 1989; Bouchaud and Georges, 1990; Schirmacher, 1991; Sahimi, 1995; Giona et al, 1996b/. This work has shown that effective macroscopic diffusivities are a function of time and space. Within a geometrically complex or disordered pore-space, the apparent diffusivity can be shown to change in the following manner

$$D_a \sim Dt^{1-2/d_w} \qquad (2\text{-}2)$$

/Muralidhar and Ramkrishna, 1993/ where D_a is the apparent diffusivity for the time-scale of observation; D is the diffusivity in water; d_w is the random walk dimension of the porous medium, which is related to the fractal dimension; and a constant of proportionality scales the relationship for units of time and for physical quantities such as porosity and sorptivity (although these properties may also be distributed heterogeneously). In a Euclidian geometry, $d_w = 2$, and D_a would be constant. However, in a three-dimensional percolation network (for example) near the percolation threshold (percolation networks are fractals near the percolation threshold), $d_w \simeq 3.8$ /Sahimi,

1993/. It can then be seen from Eqn. (2-2) that D_a would change approximately as $t^{-1/2}$. Also see Figure 3-1 and associated discussion in Section 3-1.

Similar relationships show that the apparent diffusivity also scales with inverse distance. In general, the diffusivity can be shown to decrease over any length scale less than the correlation length. In fractal media, the correlation length is infinite and therefore the diffusivity is inherently scale-dependent over any range of scales. For example, it can be shown that the diffusivity scales as $L^{-1.8}$ in a 3-D percolation network at the percolation threshold /e.g., Sahimi, 1995/ where the diffusivity is measured across distance L. However, disordered media that are non-fractal will also have scale-dependent diffusivity over any range of scales smaller than the correlation length.

Other work /Avnir et al, 1984; Turcotte, 1986; Thompson et al, 1987; Krohn, 1988; National Research Council, 1996; Aharonov et al, 1997; Delascuevas, 1997/ suggests that the pore-space of many natural materials (both fractured and porous) is well-described as fractal. Katz and Thompson /1985/ found that a particular sandstone had a fractal dimension of 2.57-2.87 that extended down to 10 Å. Delascuevas /1997/ found that the pore-surface structure of both the macro- and micro-pores within natural rock salt were fractal. If the pore space is a fractal, then Eqn. (2-2) holds over all times, whereas if the pore space is "fractal-like" over some finite volume range, then Eqn. (2-2) holds up to some t_{max}, after which D_a becomes a constant. However, well-test and rock mechanics literature suggests that the pore-space of many fractured media are well-described as fractals to very large volumes of rock /e.g., Ghosh and Daemen, 1993 Acuna and Yortsos, 1995/.

In many natural materials, therefore, the apparent diffusivity must decrease as a function of observation (experimental) time or distance. Consequently, it is possible that apparent diffusion or mass transfer coefficients decrease by several orders of magnitude from short-duration experiments (hours to weeks) to long-duration field-scale transport (weeks to decades or longer). In media with very large immobile zones (such as fractured media with large matrix blocks), it is possible (but unknown) that diffusivities could continue to change for much longer time periods (i.e., centuries or more).

2.1.1 A physical explanation for anomalous diffusion

A physical explanation for apparent diffusivities that change as a function of time within geometrically complex pore spaces is as follows. If molecules are placed at a given point within a three-dimensional, geometrically simple (i.e., Euclidian) pore space such as a sphere, it is well-known /e.g., Hughes, 1994; Sahimi, 1995/ that Fick's law holds and the mean-square displacement of those molecules is given by (in 3D):

$$\left\langle R^2(t) \right\rangle = 6Dt \tag{2-3}$$

where $R(t)$ is the displacement of a molecule from its origin over time t. Within a Euclidian geometry, the molecules are free to diffuse any distance in any direction allowed by the dimensionality of the geometry (i.e., 1, 2, or 3).

Within a geometrically complex pore-space, such as a fractal porous medium, diffusion also begins in a similar manner. However, as diffusion progresses, the molecules begin to run into "dead ends". Once a molecule is within a dead-end, and before $R(t)$ can

increase again, the molecule must diffuse back to the branch-point[1] where the dead-end path began. Then the molecule must diffuse down another pathway, which may or may not lead to another dead-end. From a macroscopic perspective, this results in diffusion that appears to slow through time. Dead ends may be in the form of molecular-sized, individual pores, or may be in the form of large numbers of interconnected pores that as a group comprise a dead end. A true fractal will contain dead ends at all spatial scales. Therefore, Fick's law does not hold, diffusion is anomalous, and the mean-square displacement grows sub-linearly:

$$\left\langle R^2(t) \right\rangle \sim t^{2/d_w} \tag{2-4}$$

/e.g., Havlin and Ben-Avraham, 1987/. Consequently, the apparent diffusivity appears to decrease through time. For this type of system, Bouchaud and Georges /1990, p. 131/ make two important statements,

> *"Since the usual laws of Brownian motion result from the central limit theorem... the usual form of these laws (i.e., the diffusion equation) has to fail whenever anomalous diffusion occurs."*

and

> *"All... effective-medium approximations which attempt to replace the disordered system by an equivalent ordered one following some averaging technique can only fail when anomalous diffusion takes place."*

Therefore, it is imperative for solute transport in fractured media to determine when anomalous (non-Fickian) diffusion is important, and to determine how best to predict its effects.

The primary consequences of anomalous diffusion, from the perspective of nuclear waste disposal, is a decrease in the apparent diffusivity through time. In other words, the apparent diffusivity is no longer only a function of the solute and the rock, but also of observation time. If anomalous diffusion applies over large ranges of time and space, then the measured apparent diffusivity is only applicable over the same space- and time-scale that the diffusivity was measured. Application of the diffusivity over a longer time-scale will result in over-prediction of diffusion into the rock and consequent under-prediction of the transport velocity.

An alternative, but equivalent, viewpoint is that the apparent diffusivity is a function of the connectivity of the pore-space. Lower connectivity leads to a lower apparent diffusivity. If the rock is less connected with distance at the matrix scale (i.e., between fractures), then the diffusivity decreases with distance (sample size). The danger is that the relatively high connectivity of the small laboratory sample is applied (de facto) to the much larger field-scale problem; however, the connectivity of the matrix at the field-scale may be unknown.

---

[1] Statistically, this increases the probability that the molecule will be released back to the fracture and then advected further down-gradient. If the medium were "well-connected" and Euclidian, the molecule would have a lower probability of being released back to the fracture.

2.1.2 Consequences of anomalous diffusion for nuclear waste disposal

If anomalous diffusion occurs within rock, the most important physical and modeling consequences for nuclear waste disposal are summarized as below.

1. No single value of diffusivity can represent the diffusion process at all time- or length-scales. Expressed in another manner, any single diffusivity is representative of diffusion only at one time- or length-scale.

2. The diffusivity decreases with both time- and length-scale of measurement. The mean diffusivity for true anomalous diffusion approaches zero at very large time- or length-scales (i.e., the pore space at very large distances is very poorly connected).

3. The porosity of the matrix may not be entirely accessed by a solute diffusing through the pores. Some fraction of the porosity may remain inaccessible via aqueous diffusion for all time.

4. Given a model of diffusion using a single diffusivity, some fraction of the porosity will be accessed less quickly than a Fickian model of diffusion would predict.

5. Laboratory measurements using the through-diffusion approach (e.g., Skagius and Neretnieks, 1986) will yield diffusivities that decrease with sample length.

6. Laboratory measurements that allow diffusion in and out of the same surface and that depend on the tail concentration for an estimate of diffusivity (e.g., column experiments, purge experiments, batch “desorption” experiments) will yield diffusivities that decrease with experimental time (assuming a single diffusivity is estimated).

7. A transport model incorporating advection and matrix diffusion and that assumes the total matrix porosity is accessible by diffusion will over-estimate the late-time retardation of the solute plume. Performance Assessment transport calculations would therefore be non-conservative.

2.2 Multirate diffusion

Multirate diffusion refers to the idea that within a small volume of rock (relative to the transport scale) there exist multiple time-scales of diffusion (or, alternatively, the inverse of time-scales, which are diffusion rate coefficients) that operate simultaneously. These varying time-scales may be due to variability within (1) matrix block size; (2) pore geometry (tortuosity, cross-sectional area, and connectivity); and (3) sorption capacity and strength /Haggerty and Gorelick, 1995, 1998/. As such, the concept includes anomalous diffusion, but is not restricted only to anomalous diffusion.

As applied in the literature to date, multirate diffusion typically invokes diffusion between an advection-dominated (“mobile”) zone and a diffusion-dominated rock matrix (“immobile zone”) that is heterogeneous at the pore-scale. The multirate diffusion model /Haggerty and Gorelick, 1995, 1998/ is essentially a modified double-porosity model /e.g., Neretnieks, 1980, 1993/ consisting of advective porosity and diffusive porosity, with diffusion of mass from one to the other described by a range of

rate coefficients[2]. There is now a growing body of literature documenting the existence, observability, and effects of multiple rates of mass transfer on solute transport in the subsurface. Multiple rates of diffusive or sorptive mass transfer are theoretically and intuitively reasonable /e.g., Ruthven and Loughlin, 1971; Villermaux, 1981; Rao et al, 1982; Cooney et al, 1983; Neretnieks and Rasmuson, 1984; Rasmuson, 1985, 1986; Fong and Mulkey, 1990; Valocchi, 1990; Lafolie and Hayot, 1993; Haggerty and Gorelick, 1995; Cunningham et al, 1997/, and have now been observed and modeled in a number of laboratory experiments /e.g., Ball and Roberts, 1991; Rate et al, 1992; Connaughton et al, 1993; Backes et al, 1995; Pedit and Miller, 1994, 1995; Chen and Wagenet, 1995, 1997; Culver et al, 1997; Werth et al, 1997; Haggerty and Gorelick, 1998; Lorden et al, 1998; and others[3]/. Haggerty et al, 1998 /in revision/ and McKenna et al /in review/ apply the concept to field-scale transport at the WIPP Site.

As with anomalous diffusion, the primary consequences of multirate diffusion, from the perspective of nuclear waste disposal, is a decrease in the apparent diffusivity through time. Again, the apparent diffusivity becomes a function of the experimental observation time as well as the properties of the solute and the rock. If multirate diffusion applies over many different time-scales, then the measured apparent diffusivity is only applicable over the same time-scale that the diffusivity was measured. Also see Figure 3-1 and associated discussion in Section 3.1.

Unlike anomalous diffusion due to a fractal pore-geometry, however, it is possible in many cases to calculate an effective or average apparent diffusion rate coefficient for some multirate diffusion cases. Whether or not such an average rate coefficient can be calculated depends on the nature of the distribution of diffusion time-scales. Any distribution of diffusion time-scales with a non-infinite arithmetic mean will allow an effective rate coefficient to be used. However, for that effective rate coefficient to be known requires an experiment of at least the mean diffusion time. Any experiment conducted over a shorter duration will result in a rate coefficient that is a function of experimental observation time. See Section 6 for further discussion, and particularly Section 6.3.

2.2.1 Consequences of multirate diffusion for nuclear waste disposal

The consequences of multirate diffusion are identical to those of anomalous diffusion (since the concept of multirate diffusion can include anomalous diffusion), but with the following exceptions.

1. Through-diffusion measurements may not yield diffusivities that decrease with sample length. This is because pores and pore networks with different diffusivities

---

[2] Note that by "rate coefficient" we mean either a first-order rate coefficient (α) used in a linear driving force model or a diffusion rate coefficient (D_a/a^2) used in a model that explicitly defines the geometry into which diffusion occurs. Any transport model with diffusion into an assumed non-infinite matrix block size ultimately uses a rate coefficient as a fundamental parameter. Although D_a and a^2 may be defined separately, changing D_a is precisely equivalent to changing a^{-2} by the same factor.

[3] Note that a large number of papers in physical chemistry have been devoted to the concept of "dispersed kinetics", or distributed rates of reaction and evidence for such distributed rates /e.g., Alberty et al, 1985; Sworakowski and Nespurek /1998/. It is reasonable to assume that surface sorption is subject to such distributed rates /e.g., Rate et al, 1992; Hu and Do, 1994; Backes et al, 1995, Wang and Do, 1999, and many others/.

may each span the length of all samples. In this case, the estimated diffusivity will tend to be dominated by the largest values of diffusivity[4].

2. Multirate diffusion would not necessarily prevent diffusion from accessing all pore space. However, it is still true that given a model of diffusion using a single diffusivity, some fraction of the porosity will be accessed less quickly than a single-rate model of diffusion would predict.

3. Over some range of times, no single value of diffusivity can represent the diffusion process. However, provided that the distribution of Da/a2 has a non-zero harmonic mean, then a single value of diffusivity can represent the diffusion process at long enough time (see Section 6.3.1).

[4] By analogy with pressure diffusion parallel to layers of varying permeability (or thermal conduction parallel to layers of varying thermal conductivity), the diffusivity estimated in through-diffusion experiments in media with non-intersecting pore-networks will be approximately the *arithmetic mean*. A similar analogy for a lognormal distribution of diffusivities that are spatially random and connected together will yield an estimate close to the *geometric mean*. However, it can be shown that the correct mean diffusivity or diffusion rate coefficient to use in transport is the *harmonic mean* (see, for example, Cunningham and Roberts /1998/ or Section 6.1.4). Since the arithmetic and geometric means are always greater than (or equal to) the harmonic mean, through-diffusion experiments will generally yield estimates of diffusivity that are larger than should be used for transport calculations.

3 Evaluation of existing data and assessment of potential for anomalous or multirate diffusion

In this section we provide an overview of our analysis of evidence for multirate and anomalous diffusion. We focus on Fenno-Scandian granitic rocks, with the exception of Section 3.1, in which other data were also considered.

3.1 Observation-time-dependence of rate coefficients

To examine the issue of time-dependent rate coefficients, we compiled a number of studies where rate coefficients were estimated from batch, column, and field tracer tests. The results from our literature search are displayed in Figure 3-1. The estimated rate coefficient is plotted on the vertical axis, and the duration of the experiment on the horizontal axis. Data from 100 experiments are shown. We see that, in general, large rate coefficients, which represent fast mass transfer, are estimated from short experiments. Similarly, small rate coefficients, which represent slow mass transfer, are estimated from long experiments. As a general trend, the longer the duration of the experiment, the slower is the estimated rate of mass transfer. In a fashion similar to the well-known Figure 3-2 of Gelhar et al /1992, p. 1968/, showing dispersivity vs. spatial scale of measurement, we see that the parameter of interest appears to be a function of the experimental design from which the parameter is estimated. In our case, however, the scale is time rather than space.

A longer-duration experiment in the same porous medium is likely to experience apparently slower mass transfer, while a shorter-duration experiment is likely to experience apparently faster mass transfer. Thus, we hypothesize that a model using a single rate coefficient (either first-order or diffusion) to represent mass transfer will only be valid at the same time-scale as the experiment from which the rate coefficient is estimated. To produce an accurate prediction of solute transport for any time-scale other than that of the original experiment, we must know what rate coefficient will dominate at the time-scale of our prediction.

When interpreting Figure 3-1, it should be remembered that we have not considered changes in experimental design factors such as pore-water velocity, injection time, and so forth, that will result in changes in the estimated rate coefficient. Young and Ball /1995/ have shown that rate coefficients change through time if the mass transfer model is mis-specified. Pore-water velocity has been experimentally confirmed as having an important effect on the estimated rate coefficient /Brusseau, 1992; Li et al, 1994; Griffioen et al, 1997, 1998/.

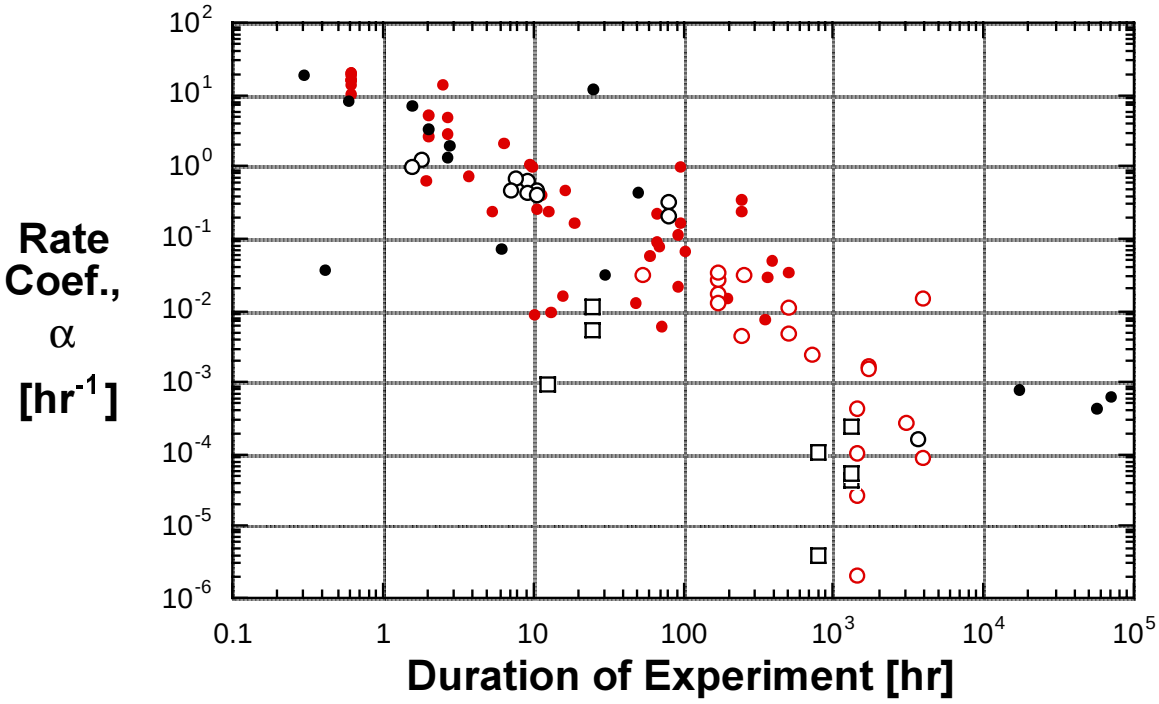

Figure 3-1. *Rate coefficients for 100 laboratory and field from the literature, graphed versus the time-scale of the experiment where they were measured. The rate coefficient is either a first-order rate coefficient (i.e., α) or a diffusion rate coefficient (i.e., D_d/a^2). Where a diffusion rate coefficient is shown, it is multiplied by 15 if the assumed geometry is a spheres and by 3 if the assumed geometry is a layer. The multiplication factor makes the rate coefficients approximately equivalent in that the mean residence times are the same /after Glueckauf, 1955 or Goltz and Roberts, 1986; also see Section 6.1.4/.*

- Unconsolidated: Sorbing solute: First-order rate coefficient
- Unconsolidated: Non-sorbing solute: First-order rate coefficient
- o Unconsolidated: Sorbing solute: Diffusion rate coefficient
- o Unconsolidated: Non-sorbing solute: Diffusion rate coefficient
- □ Unconsolidated: Non-sorbing solute: First-order rate coefficient

3.2 Through-diffusion experiments

Two of the signatures of anomalous diffusion are time- and scale-dependent diffusivities (depending on the type of measurements taken). In particular, in fractal media, it can be shown that the diffusivity will scale as L^{2-d_w}, where L is the dimension of the sample across which diffusivity is measured and d_w is the random walk dimension of the rock. The value of the random walk dimension changes as a function of the pore geometry in the rock. However, if the pore-space has the characteristics of a fractal, the value will always be greater than 2. It can be shown analytically that in a 3-D percolation network at the percolation threshold (i.e., a porous medium just at the threshold of being "self-connected"), that the random walk dimension is approximately 3.8 /Sahimi, 1995/. In media that are not true fractals, but that have significant disorder over several length-scales, it can be expected that diffusivity will also decrease with sample length;

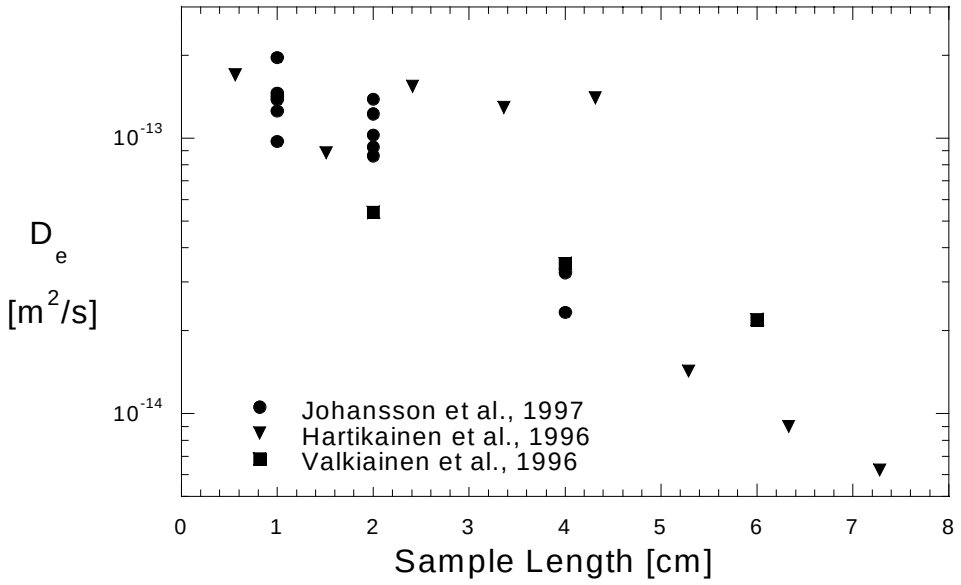

Figure 3-2. *Effective diffusivities in three Finnish and Swedish granitic rocks.*

however, the exact nature of the decrease cannot be predicted without a more detailed knowledge of the pore-scale geometry of the rock.

A review of diffusion in Fenno-Scandian granitic rocks turned up three experiments conducted over different length-scales in similar granitic materials that show the type of apparent anomalous behavior discussed above. Figure 3-2 shows effective diffusivities vs. sample length for these three experiments, all conducted in Swedish and Finnish granitic rocks /Johansson et al, 1997; Hartikainen et al, 1996; and Valkiainen et al, 1996/. Two of the sets of experiments were conducted with tritiated water (HTO), and one set was conducted with helium gas (the values of D_e have been converted to equivalent HTO diffusivities).

Other work by Skagius and Neretnieks /1986, p. 19/ showed that the formation factor decreased as a function of length of the rock sample. However, in their work it was found the decrease ceased after approximately 30 mm. This is evidence against anomalous diffusion, though diffusivity would still appear to be time-varying as long as the depth-of-penetration were less than 30 mm.

3.3 Laboratory sorption and diffusion experiments

From the perspective of transport of a sorbing solute, and within the multirate diffusion framework, the function of interest is the distribution of the diffusion rate coefficient (i.e., its density function). In detail, this parameter is:

$$\frac{D_a}{a^2} = \frac{D_p}{\left(1 + \frac{\rho K_d}{\phi}\right) a^2} = \frac{D\delta_D}{\tau^2 \left(1 + \frac{\rho K_d}{\phi}\right) a^2} \tag{3-1}$$

where D_p [L^2/T] is the pore diffusivity; D [L^2/T] is the aqueous diffusivity; δ_D [-] is the constrictivity; τ^2 [-] is the tortuosity; ρ [M/L^3] is the bulk density; K_d [L^3/M] is the distribution coefficient, ϕ [-] is porosity; and a [L] is the distance into the rock to which the pore or pore network is connected. Within the diffusion rate coefficient there are three parameter groups that may vary significantly: pore diffusivity, the retardation factor, and the length scale (a). If each of these vary by one order of magnitude and if they are somewhat independent of each other, then the diffusion rate coefficient varies by approximately four orders of magnitude (remembering that a is squared). Additionally, since the variations are multiplicative, we would expect that (or at least not be surprised if) the resulting distribution is lognormal.

Ideally, we would like to know the density function $b(D_d/a^2)$ from each of the components of D_d/a^2. At present, this is not possible due to lack of data (it is unlikely ever to be possible, in fact). However, it may be possible to place some boundaries on the distribution given current knowledge.

Laboratory diffusion experiments in granitic rocks have been reviewed in detail by Ohlsson and Neretnieks /1995, 1997/. In their review of diffusion in Fenno-Scandian granitic rock, they found that the apparent diffusivity of tritiated water (HTO)[5] D_p, varies over approximately 2 orders of magnitude, from approximately 5.5 x 10^{-10} m^2/s to 7.8 x 10^{-12} m^2/s. It may be that the variability within a repository is less than this entire range, but such a range would likely form a maximum estimate of the total range of variability over the length-scales measured (currently up to several cm). As a conservative estimate, let us assume the variability ranges over a factor of 10.

A number of laboratory sorption experiments were conducted by Byegård et al /1998/. Experiments were conducted with Na, Ca, Rb, Sr, Cs, and Ba on nine different Äspö rock samples (as well as other individual mineral samples, etc.) Minimum and maximum values of K_d are as follows, where values are taken from the longer-term experiments (e.g., 7–36 days) and larger grain sizes (e.g., 1–2 mm):

Table 3-1. Table showing minimum and maximum K_d values measured by Byegård et al /1998/.

	Min K_d (m^3/kg)	Max K_d (m^3/kg)	Max K_d/ Min K_d
Na	1.1 x 10^{-6}	8.0 x 10^{-6}	7.3
Ca	1.2 x 10^{-5}	8.3 x 10^{-5}	6.9
Rb	1.2 x 10^{-4}	2.8 x 10^{-3}	23
Sr	1.4 x 10^{-5}	1.1 x 10^{-4}	7.9
Cs	3.5 x 10^{-4}	5.3 x 10^{-2}	150
Ba	1.9 x 10^{-4}	1.8 x 10^{-3}	9.5

[5] Note that D_a, given by Ohlsson and Neretnieks /1995, 1997/ is approximately equivalent to D_p for HTO if surface diffusion and differences between transport and total porosity are neglected.

The average variability in K_d for individual species, excluding Cs, is approximately 10. It is reasonable to assume that based on a limited number of samples, Byegård et al /1998/ did not exhaust the variability in K_d within Äspö rock. Therefore, we take a factor of 10 to be a conservative estimate of typical variability in K_d. Given the values of K_d, this also results in a factor of 10 variability in the retardation factor for larger K_d.

The variability in *a* (the distance into the rock to which the pore or pore network is connected) is difficult to estimate. Its maximum value is bounded by approximately one-half the maximum fracture spacing (i.e., the maximum matrix half-block size), and its minimum is, of course, zero. This variability depends not only on the matrix block size, but also the pore-connectivity. As such, this is a difficult parameter to estimate. As a minimum, the variability is certainly greater than an order of magnitude, although it could be many orders of magnitude.

Examining the cumulative variability in D_d/a^2, we see that both D_p and retardation factor range over at least a factor of 10 (at least for larger K_d). Similarly, the value of a likely ranges over at least a factor of 10 (at least for larger K_d). Similarly, the value of a likely ranges over at least a factor of 10, and possibly much more. ***A conservative estimate of the variability in D_d/a^2 is therefore 10^4, or four orders of magnitude.*** If the distribution were lognormal, such variability would be represented by a standard deviation in $\ln(D_d/a^2)$ in the range of 4 to 5 (i.e., 4σ, covering 95% of the distribution and where σ = 4.6, would represent a spread of 10^4). Such a range is certain to have a significant impact on solute transport[6].

3.4 Field tracer experiments

Without constructing a flow and transport model for each tracer experiment that includes multirate diffusion as a hypothesis, it is difficult to rule out or demonstrate multirate diffusion. However, in some cases the signature of multirate diffusion may be apparent. In particular, the following provide clues that multirate diffusion may be a factor in the proper interpretation of tracer data:

1. Tracer tests conducted over different time-scales (either by changing the fluid velocity or transport distance) yield different estimates of mass transfer parameters (diffusivity, block size, and capacity coefficient);

2. Following a pulse injection of tracer, the late-time slope of the breakthrough curve (BTC) has power-law behavior (see Section 6);

3. Following a pulse injection of tracer, the tail of the BTC is particularly "fat" but not necessarily power-law.

An examination of tracer data available to us revealed none of the above phenomena that could unambiguously be attributed to multirate diffusion. One set of tracer data from Stripa /Byegård et al, 1992, Figs. 6, 7/ exhibits power-law behavior at intermediate times. However, these tests are recirculating tests and therefore late-time behavior is masked by the recirculation.

---

[6] Note that most simulations of solute transport with a lognormal distribution that have been published in the literature /e.g., Rasmuson, 1986; Valocchi, 1990/ considered much smaller σ.

Tracer data from the TRUE-1 experiments is currently being analyzed using the multi-rate approach by Henrik Johansson [Dept. of Nuclear Chemistry, Chalmers University of Technology, Göteborg] in collaboration with Oregon State University. We expect a report and paper to come from this analysis that will outline the utility or non-utility of the multirate approach in dealing with these experiments. Consequently, at this time we are unable to comment directly on the multirate concept as it reflects on the TRUE-1 data set.

4 Design of LTDE: Scoping calculations

Matrix diffusion studies of radionuclides in Swedish granitic rocks have been performed in several laboratory experiments (reviewed by Ohlsson and Neretnieks /1995/; Ohlsson and Neretnieks /1997/) and field experiments at the Stripa mine /e.g., Birgersson and Neretnieks, 1982, 1984, 1990/. A Long-Term Diffusion Experiment (LTDE) is now planned for the Äspö HRL. The preliminary test plan for the LTDE /Byegård et al, 1999/ considered both injected and natural tracers measured in a set of boreholes. The goals of the LTDE are /Byegård et al, 1999/ are as follows.

- To investigate diffusion into matrix rock in situ under natural rock stress conditions and hydraulic pressure and groundwater chemical conditions.

- To obtain data on sorption properties and processes of some radionuclides on undisturbed matrix rock and on fresh granitic rock surfaces.

- To compare laboratory derived diffusion constants and sorption coefficients for the investigated host rock with the sorption behaviour observed in situ at natural conditions, and to evaluate if laboratory scale sorption results are representative also for larger scales.

- To evaluate the impact of heterogeneous diffusion (i.e., both anomalous and multirate).

For the purpose of assisting with this preliminary design, a series of scoping calculations were undertaken. The results of these scoping calculations are reported here.

Following the completion of our scoping calculations, two additional LTDE designs were considered /Winberg, 1999/, for which no scoping calculations are reported here.

4.1 Solute transport code

We wrote a series of four solute transport codes to model advection, dispersion, and diffusion radially away from a well. The codes are modifications of STAMMT-L /Haggerty and Reeves, 1999/, which models 1-D solute transport in the presence of rate-limited mass transfer. The modified versions of this code perform the functions listed below. The name in brackets refers to the version of the code performing the function. Note that STAMMT-L SKB4 is capable of all 4 functions.

1. Homogeneous, radial diffusion into a finite cylindrical matrix. Calculates concentration histories at an injection well only. Rock matrix may initially contain tracer or be tracer-free. (STAMMT-L SKB1).

2. Homogeneous, radial diffusion into a finite cylindrical matrix. Calculates concentration histories obtained at both the injection well and an observation well. The observation well is located at the edge of the finite matrix. Rock matrix may initially contain tracer or be tracer-free. (STAMMT-L SKB2).

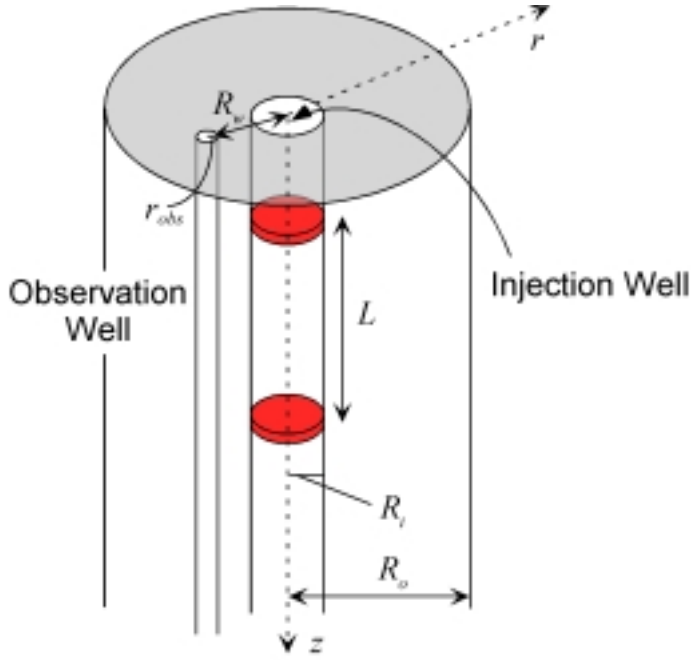

Figure 4-1. *Conceptual model for LTDE scoping calculations.*

3. Homogeneous, radial diffusion into a finite cylindrical matrix. In addition to the concentration histories of SKB2, this code calculates a concentration profile between the injection and observation wells. Rock matrix may initially contain tracer or be tracer-free. (STAMMT-L SKB3).

4. Heterogeneous, radial diffusion into a finite cylindrical matrix. Assumes a log-normal distribution of D_a (see Section 4.1.1 Code verification). Calculates concentration histories in the injection well. Rock matrix may initially contain tracer or be tracer-free. (STAMMT-L SKB4).

A drawing of the conceptual model for the scoping calculations is shown in Figure 4-1.

4.1.1 Mathematical model, homogeneous rock

Mathematical overview:

The transport equations for advection, dispersion, and radial diffusion are

$$\frac{\partial c}{\partial t} = \frac{D_L}{R_a}\frac{\partial^2 c}{\partial z^2} - \frac{v_z}{R_a}\frac{\partial c}{\partial z} - \beta_{tot}\frac{\partial \hat{c_m}}{\partial t} \tag{4-1}$$

$$\frac{\partial c_m}{\partial t} = \frac{D_a}{r}\frac{\partial}{\partial z}\left(r\frac{\partial c_m}{\partial r}\right) \tag{4-2}$$

where all variables are defined in the Appendix (Section 9). The transport equations are coupled by

$$\hat{c_m} = \frac{2}{R_o^2 - R_i^2}\int_{R_i}^{R_o} r c_m dr \tag{4-3}$$

The boundary and initial conditions on the advection-dispersion equation are

$$\pi R_i^2 D_L \frac{\partial c\left(z = 0\ ,\ t\right)}{\partial z} - Qc\left(z = 0\ ,\ t\right) = Qc_b \tag{4-4}$$

$$\frac{\partial c\left(z = L\ ,\ t\right)}{\partial z} = 0 \tag{4-5}$$

$$c\left(z\ ,\ t = 0\right) = c_0 \tag{4-6}$$

The boundary and initial conditions on the diffusion equation are

$$c_m\left(r = R_i\ ,\ t\right) = c \tag{4-7}$$

$$\frac{\partial c_m\left(r = R_o\ ,\ t\right)}{\partial r} = 0 \tag{4-8}$$

$$c_m\left(r,\ t = 0\right) = c_0 \tag{4-9}$$

For all equations, see Section 9 for variable definitions. The equations may be nondimensionalized using the following transforms /following van Genuchten et al, 1984/:

$$\tau = \frac{v_z t}{R_a L} \tag{4-10}$$

$$Z = \frac{z}{L} \tag{4-11}$$

$$P = \frac{v_z L}{D_L} \tag{4-12}$$

$$\xi = \frac{r}{R_i} \tag{4-13}$$

$$\xi_o = \frac{R_o}{R_i} \tag{4-14}$$

$$\lambda = \frac{D_a R_a L}{R_i^2 v_z} \tag{4-15}$$

Using these variable transforms, we "nondimensionalize" the transport equations and then take the Laplace transform of all equations. We then solve the diffusion equation and substitute that solution back into the advection-dispersion equation. The advection-dispersion equation becomes

$$\left(s\bar{c} - c_0\right)\left[1 + \frac{2\beta_{tot} M(\omega)}{\omega\left(\xi_o^2 - 1\right) N(\omega)}\right] = \frac{1}{P}\frac{\partial^2 \bar{c}}{\partial Z^2} - \frac{\partial \bar{c}}{\partial Z} \tag{4-16}$$

where

$$\omega = \left(\frac{s}{\lambda}\right)^{1/2} \tag{4-17}$$

$$M(\omega) = I_1(\omega\xi_o)K_1(\omega) - I_1(\omega)K_1(\omega\xi_o) \tag{4-18}$$

$$N(\omega) = I_0(\omega)K_1(\omega\,\xi_o) + I_1(\omega\,\xi_o)K_0(\omega) \tag{4-19}$$

Noting that the rational term on the left-hand-side of (4-16) is a constant for the purposes of solution in the Laplace domain, this equation is straightforward to solve, and has been solved by various authors, including Haggerty and Gorelick /1998/.

The concentration in the matrix away from the injection well is /after van Genuchten et al, 1984/

$$\overline{c_m} = \bar{c}\,\frac{I_0(\omega\xi)K_1(\omega\xi_0) + I_1(\omega\xi_0)K_0(\omega\xi)}{I_0(\omega)K_1(\omega\xi_0) + I_1(\omega\xi_0)K_0(\omega)} \tag{4-20}$$

The concentration in an observation well is given by the solution of

$$\frac{\partial c_{obs}}{\partial t} = \frac{\textit{well area} \perp \textit{to diffusion}}{\textit{well volume}}\, J \cong -\frac{2\phi D_a}{\pi r_{obs}}\frac{\partial c_m}{\partial x} \tag{4-21}$$

In the Laplace domain and in dimensionless notation, (4-21) becomes

$$\overline{c_{obs}} = \frac{2\phi R_i}{\pi r_{obs}\omega}\,\bar{c}\,\frac{I_1(\omega\xi_0)K_1(\omega\xi) - I_1(\omega\xi)K_1(\omega\xi_0)}{I_0(\omega)K_1(\omega\xi_0) + I_1(\omega\xi_0)K_0(\omega)} \qquad (4\text{-}22)$$

Code Verification:

The STAMMT-L-SKB4 code (containing all options) was first checked for consistency in terms of mass balances, breakthrough times, penetration depths for diffusion away from the well, and tailing due to diffusion in the breakthrough curves.

The code then was quantitatively verified against van Genuchten et al's /1984/ solution. The verification was informal in that STAMMT-L-SKB4 was visually compared the van Genuchten et al solution as given in Figures 3-2 and 4-1 of their paper (p. 344), which was scanned into a data extraction program. The parameters used in the verification simulation were D_L = 4.9 x 10^{-5} m^2/s; D_a = 3.7 x 10^{-2} m^2/s; L = 0.404 m; v_z = 4.9 x 10^{-3} m/s; R_i = 7.3 x 10^{-4} m; R_o = 1.18 x 10^{-2} m; and ϕ = 0.6819. Both the breakthrough curves and the concentration profiles (3, 10, and 100 min) were compared. The detailed parameter set is given in the accompanying annotated Excel spreadsheet (encldisc.xls) with the run-names vgck-btc, vgck-3m, vgck-10m, and vgck-100m. Comparisons are shown below in Figure 4-2 and Figure 4-3. It should be emphasized that comparisons are against a scanned and data-extracted image, and therefore the van Genuchten et al data points are not precise.

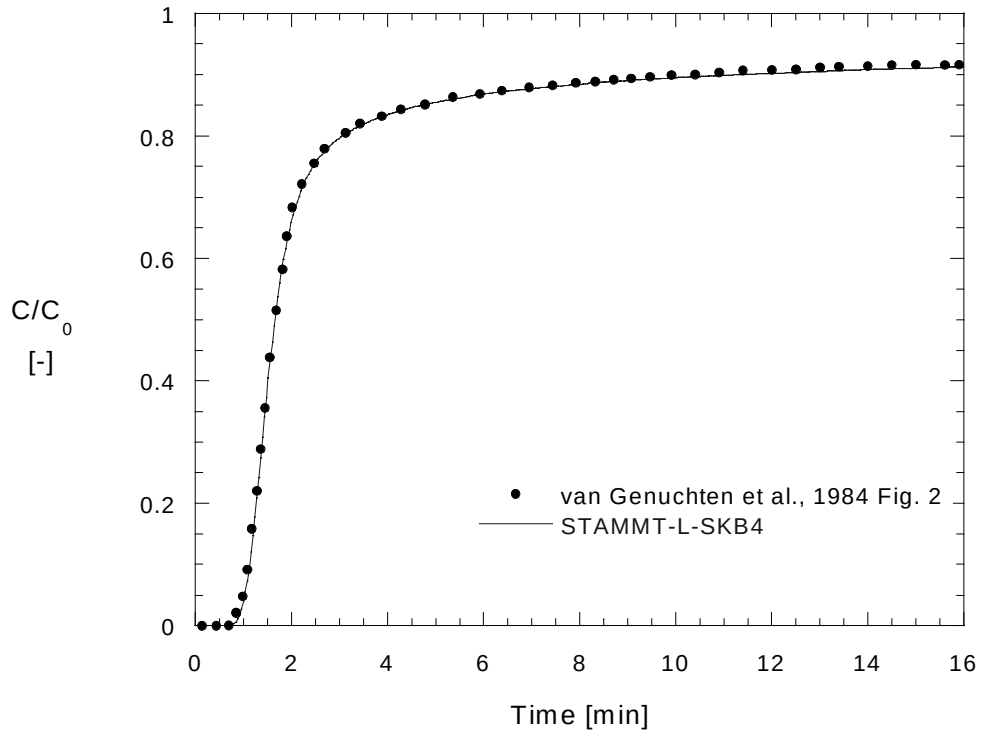

Figure 4-2. *STAMMT-L-SKB4 code breakthrough curve comparison against Figure 3-2 of van Genuchten et al /1984, p. 344/ (scanned and data-extracted).*

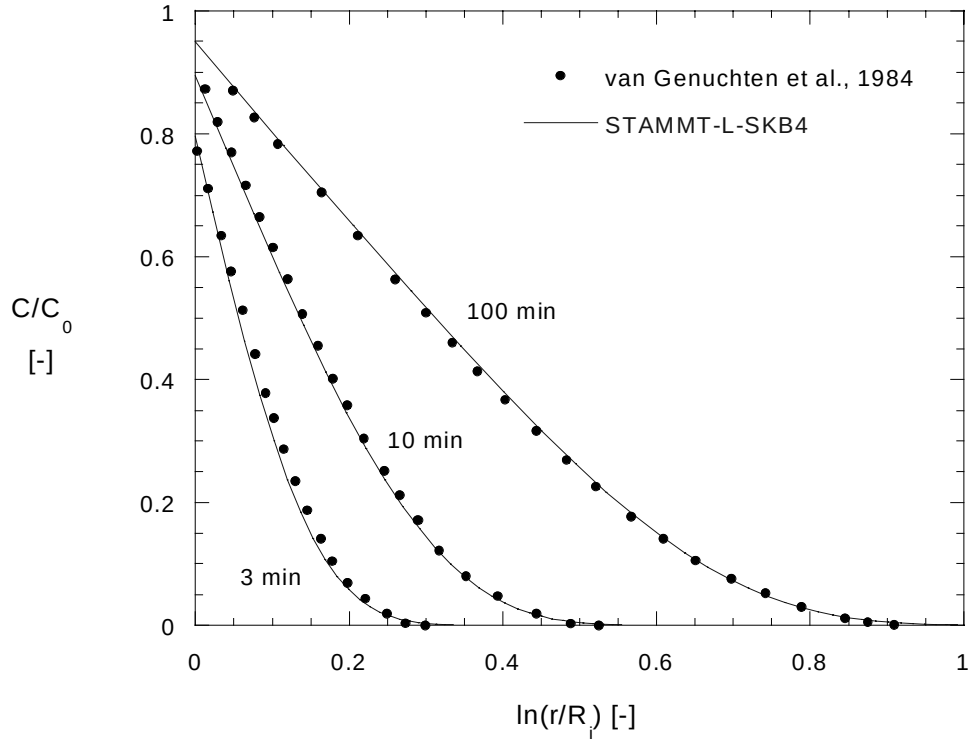

Figure 4-3. *STAMMT-L-SKB4 code concentration profiles comparison against Figure 4-1 of van Genuchten et al /1984, p. 344/ (scanned and data-extracted).*

4.1.2 Mathematical model, heterogeneous rock

To implement diffusion into heterogeneous rock we make use of the following assumptions:

1. Diffusion takes place away from the well through a distribution of non-intersecting pore-networks;

2. The geometry of any individual pore-network is radial (i.e., its cross-sectional area increases as r^2);

3. Each pore-network is characterized by a single value of D_a;

4. D_a is lognormally distributed.

5. The entire distribution of diffusivities is present at every point along the well.

We note that each of these assumptions is at best only an approximation. The 4th assumption in particular is not strictly possible because the maximum diffusivity is equal to the aqueous diffusivity (ignoring surface diffusion and other such effects). However, since diffusion in this problem scales approximately as D_a/R_e^2, where R_e is the radial distance to the end of the pore-network, the distribution is approximately equivalent to a lognormal distribution of this entire parameter group D_a/R_e^2 (similar to

the diffusion rate coefficient D_d/a^2 discussed in Section 3.3). The equivalency is not exact because diffusion in this problem depends on two length-scales, R_i and R_e; however, the dependency on the first of these is weak.

Together, the group of assumptions are not likely to be met in nature. However, the goal of the simulations, as with all simulations, is to provide a model from which to build our understanding of the influence of heterogeneous diffusivity on a radial diffusion problem. For this goal, these assumptions are reasonable.

With these assumptions, Eqn. (4-16) becomes

$$\left(s\bar{c} - c_0\right)\left[1 + \int_0^{\infty} f\left(D_a\right) \frac{2\beta_{tot} M(\omega)}{\omega\left(\xi_o^{\,2} - 1\right) N(\omega)}\, dD_a\right] = \frac{1}{P}\frac{\partial^2 \bar{c}}{\partial Z^2} - \frac{\partial \bar{c}}{\partial Z} \tag{4-23}$$

where $f(D_a)$ is the lognormal distribution:

$$f\left(D_a\right) = \frac{1}{\sqrt{2\pi}\sigma D_a} \exp\left\{-\frac{\left[\ln\left(D_a\right) - \mu\right]^2}{2\sigma^2}\right\} \tag{4-24}$$

Other definitions follow as in (4-17) – (4-19) and the ODE in (4-23) may be solved in a fashion similar to that given by Haggerty and Gorelick /1998/.

4.2 Scoping calculations

We undertook a large number of scoping calculations to help with the design of the LTDE. At the time of the work, the planned experimental design was an injection well surrounded by one or more observation wells. Both natural and injected tracers were to be used. The design allowed for one or more observation wells at various distances.

Scoping calculations were undertaken for the following scenarios:

1. Natural tracer experiments in homogeneous rock (concentration history obtained at central well only).

2. Injected tracer experiments in homogeneous rock (concentration profile obtained and concentration histories obtained at central well and observation well).

3. Natural tracer experiments in heterogeneous rock (concentration history obtained at central well only).

4. Injected tracer experiments in heterogeneous rock (concentration histories obtained at central well only).

The natural tracer is a tracer that is produced or exists in the rock naturally. An example is He, although Ar and H_2 are also possibilities. The idea with the natural tracer experiments is to flush a central well with water (ideally natural groundwater) that has had the natural tracer removed. This water is injected into the borehole, circulated there, and then pumped out at a prescribed rate. Upon exit from the borehole, either the natural tracer concentration is measured on-line or samples are taken in which the natural tracer concentrations are measured.

The injected tracer experiments are conventional experiments in that a suite of tracers is injected into the borehole and the tracers are allowed to diffuse out into the rock. In our scoping calculations it was assumed that the injection of tracer was stopped after some time. Some of the tracer diffuses out to an observation well, while some of the tracer diffuses back to the central well.

Homogeneous rock refers to rock that is homogeneous with respect to the transport parameters. In the LTDE we are dealing with transport parameters of porosity (ϕ), apparent diffusivity (D_a), and distribution coefficient (K_d). In the first sets of scoping calculations we assumed that all parameters are homogeneous. For the homogeneous scoping calculations it was assumed that the outer radius of the diffusion system was at 5.0 m, farther than the solute can reach in the time available to the LTDE.

In the second sets of scoping calculations we assumed that the apparent diffusivity is characterized by a lognormal distribution (μ, σ). Any particular diffusion "pathway" (i.e., pathway into the rock) is assumed be characterized by a single diffusivity. However, it is assumed that over the length of the borehole and around its circumference that there exists a distribution of diffusivities defined by the variables μ (log of the geometric mean apparent diffusivity) and σ (standard deviation of the log of apparent diffusivity). For the heterogeneous scoping calculations it was assumed that the outer radius of the diffusion system was 0.5 m. This assumption was made for two reason: (1) if there is heterogeneity in diffusivity but there are no dead-end pathways away from the rock, then this will yield no different effect on the concentration history at the central well (i.e., a solute diffusing out and back along a "fast" pathway looks identical to a solute diffusing out and back along a "slow" pathway if the pathways are both infinite); and (2) it is recognized that we do not know the distance to the outer radius of the diffusion system but this uncertainty is lumped into the variability assigned to the apparent diffusivity.

Scoping calculations were undertaken with a code written by Roy Haggerty for this study in October, 1998. The code is capable of simulating radial diffusion away from a well. The rock may be characterized by a single apparent diffusivity or a lognormal distribution of apparent diffusivities. Concentration histories may be obtained in the injection well or in observation wells at arbitrary distances. Concentration profiles between the injection well and arbitrary points may also be obtained. The code can deal with linearly sorbing solutes, and the solute may have different distribution coefficients along the well and in the rock. The code was tested against the solution of van Genuchten et al, 1984. Note that not all capabilities listed above may be used simultaneously – for example, it is not currently possible with the code to obtain concentration profiles for a rock with a distribution of apparent diffusivities.

All simulations to date have been conducted for non-sorbing tracers (e.g., HTO or He).

In all cases we conducted a scoping calculation for a Base Case – a set of parameters we perceive as realistic for the Äspö rocks. The parameters used in the Base Case along with the source of the parameter is shown in Table 4-1. Following a scoping calculation for the Base Case, parameters were varied for the purpose of understanding the sensitivity of the calculations to uncertainty in the parameter values.

Table 4-1. Parameters used in Base Case.

Parameter	Value	Source
Apparent diffusivity, D_a	2.0 x 10^{-11} m^2/s	/Ohlsson and Neretnieks, 1997/
Kinematic porosity, ϕ	0.005	/Ohlsson and Neretnieks, 1997/
Radius of well	0.038 m	Typical well radius at Äspö
Flushing rate of well, Q*	0.1/day	Choice
Distance to observation well (where used), R_{obs}	0.20 m	Choice based on feasibility
Concentration profile time (where used)	5 yr	Max. feasible time
Std. dev. of ln(D_a) (where used), σ	3.0	/Haggerty et al, 1998 (in revision)/
Dispersivity along well, α_L	0.01 m and 0.1 m	Arbitrary choice – unimportant parameter

The parameters listed above as well as all other parameters used in the simulations are given in an annotated Excel spreadsheet (encldisc.xls).

4.2.1 Natural tracer experiments, homogeneous rock

Several scoping calculations were conducted to investigate the potential concentration history at a well being flushed by tracer-free water, but experiencing diffusion of natural tracer from surrounding rock. In addition to the parameters listed in Table 4-1, we assumed that the outer radius of the system was at 5.0 m (beyond that region seen within 5 years) and that the well contained no dummy.

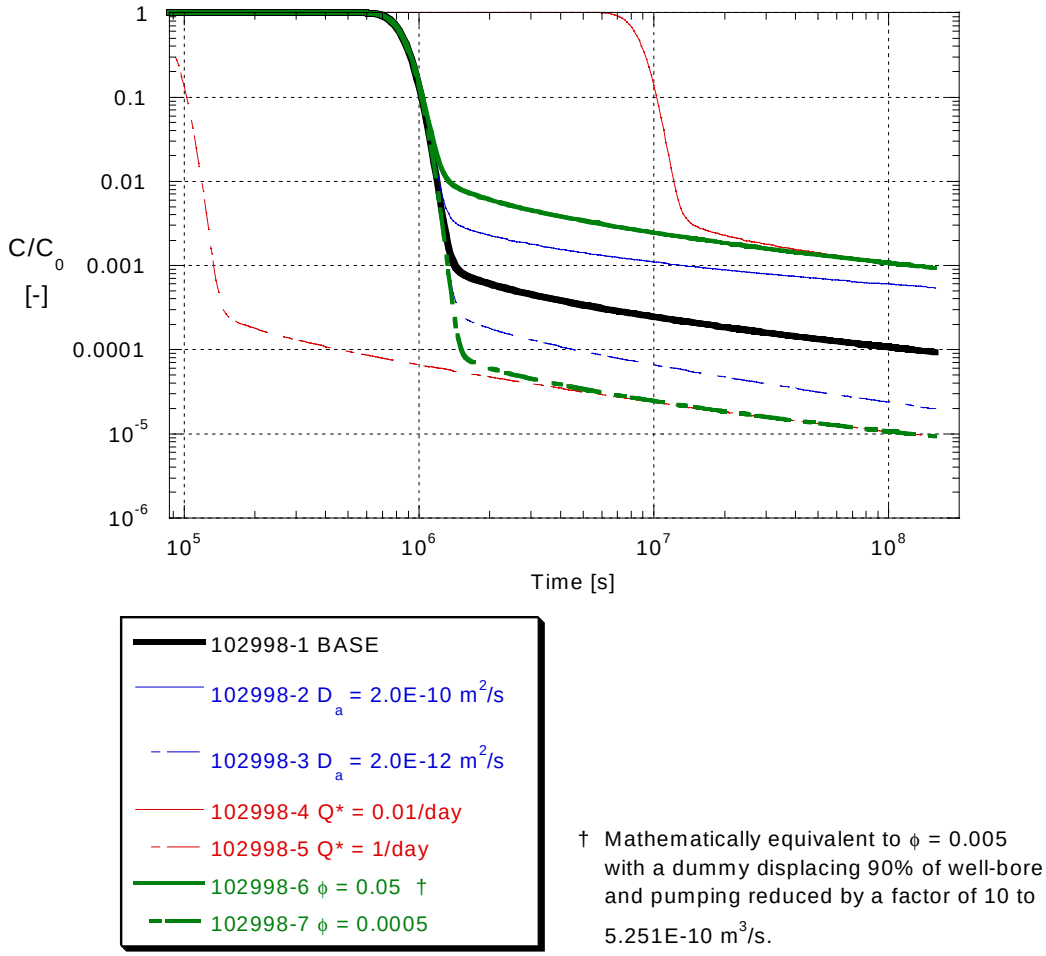

Figure 4-4. *Concentration histories at central well for natural tracer experiments in rock with homogeneous diffusivity.*

Key results for the scoping calculations for the natural tracer experiments in homogeneous rock are given in Figure 4-4. From this figure we see the type of breakthrough curves (BTCs) that we expect for the natural tracer experiments. Looking at the Base Case, we see that we can expect an initially steep decline in concentrations in the well, followed by a very long period of slow declines in concentrations. The initial steep decline occurs once the well is flushed of its initial pore-volume of water. Consequently, depending on drilling techniques, this initial phase may not occur. Following this, the rate of decrease in concentration is determined by diffusion in the rock.

From Figure 4-4 we see that the Base Case would require a dynamic range of 4 orders of magnitude if no dummy is used. If a dummy displacing 90% of the well-bore is used, and pumping is reduced to maintain a flushing rate of 0.1/day, then the curve given by $\phi = 0.05$ shows the result for the Base Case of $\phi = 0.005$. In other words, if a dummy is used, the dynamic range in concentration needed for the natural tracer is less (approximately 3 orders of magnitude in this case).

4.2.2 Injected tracer experiments, homogeneous rock

Scoping calculations were performed to investigate concentration histories in a central injection well and in an observation well for an injected tracer experiment in homogeneous rock. Concentration profiles (away from the central well) were also calculated. We again assumed that the radius of the system was at 5.0 m (beyond the region seen within 5 years) It was assumed that tracer was injected for a period of 0.5 yr. Both the observation well and the injection well are assumed to have dummies occupying 90% of the well volumes.

Figure 4-5 shows concentrations at the injection well, while Figure 4-6 shows concentrations at the observation well (R_{wobs} = 0.20 m distance, Base Case).

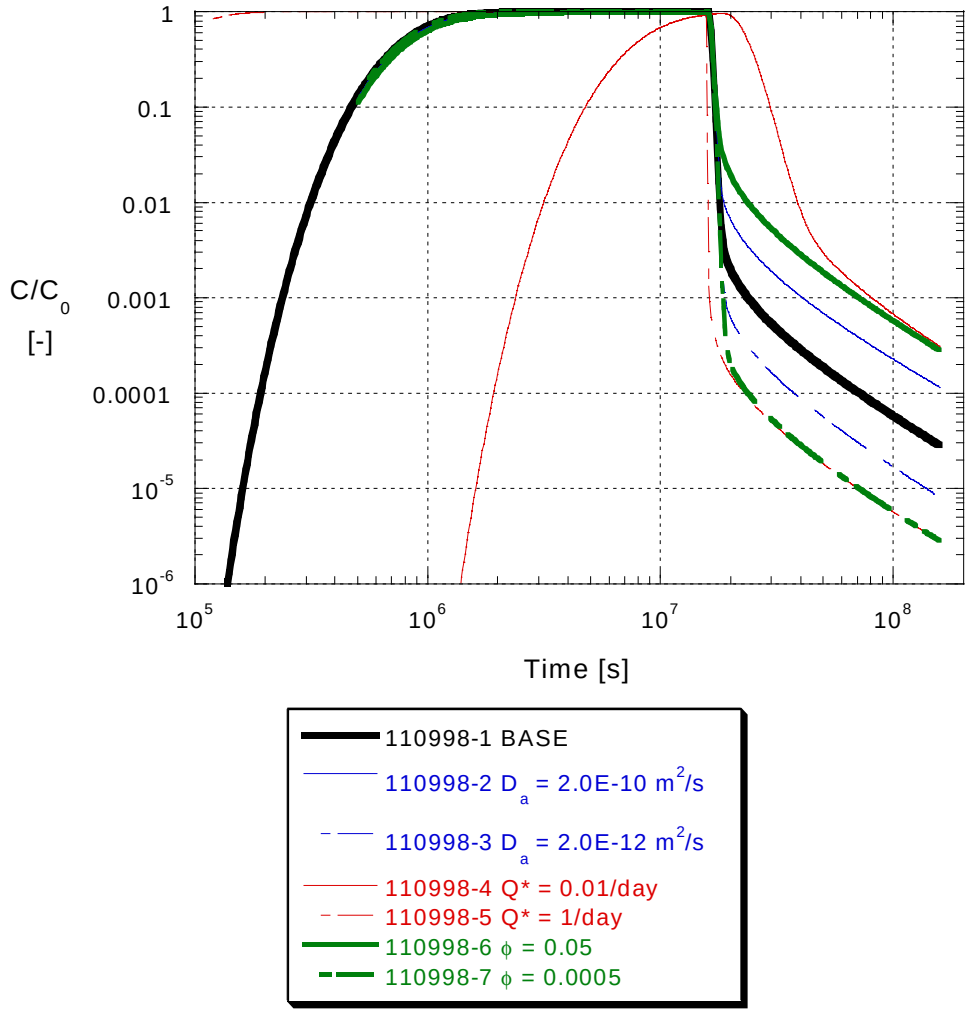

Figure 4-5. *Concentration histories at the central well for a 0.5-year injection followed by flushing with tracer-free water. Diffusivity is homogeneous.*

From these figures, several important design considerations appear in regard to concentrations. In the observation well it is apparent that 6 decades of concentration should be sufficient to obtain data over the entire duration of the experiment. However, in the observation well the needed dynamic range for tracer concentration will largely be a function of the distance to the observation well and how much the tracer is retarded. From Figure 4-6 it is clear that a distance to the observation well of 0.40 m will result in relative concentrations of less than 1 x 10^{-6} at the observation well after more than 6 years.

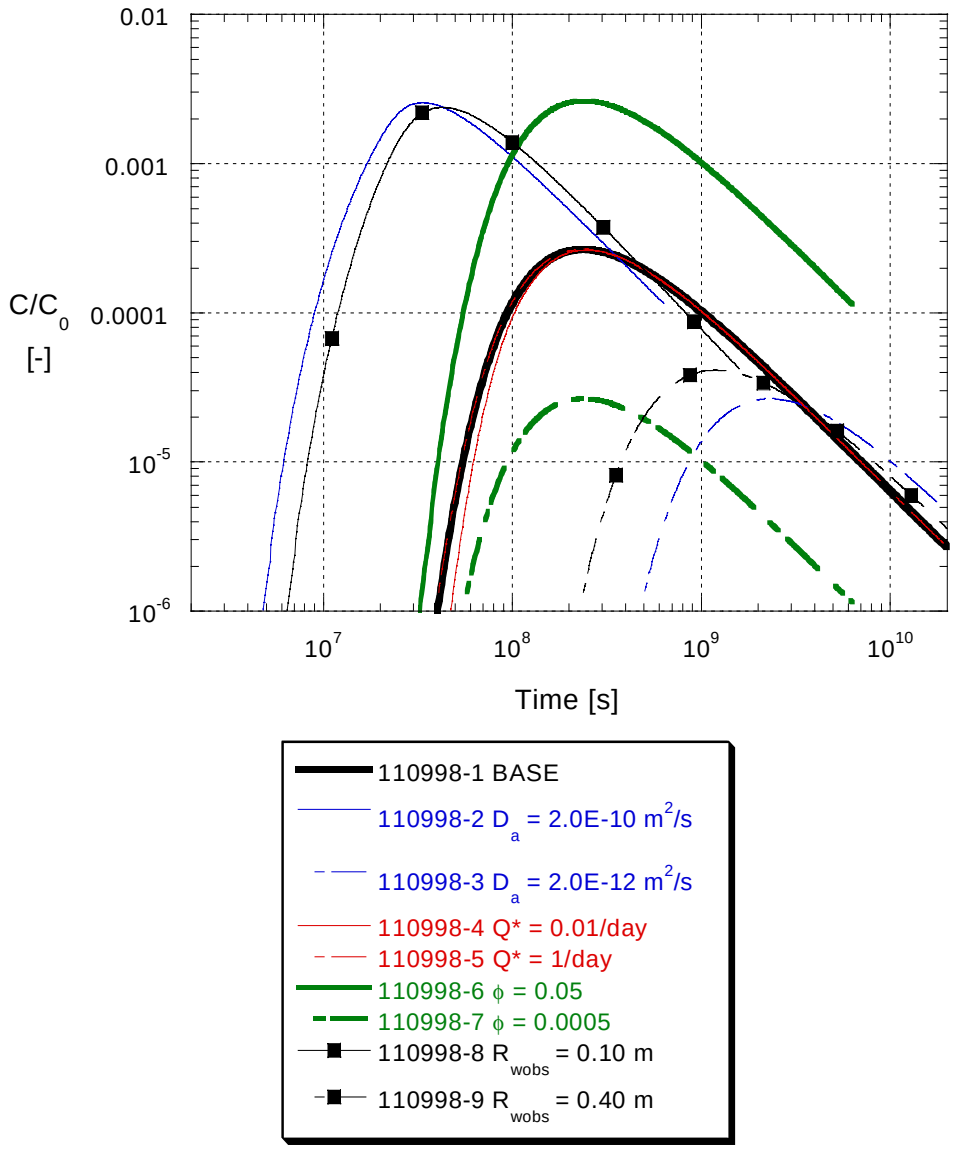

Figure 4-6. *Concentration histories for injected tracer at observation well in rock with homogeneous diffusivity.*

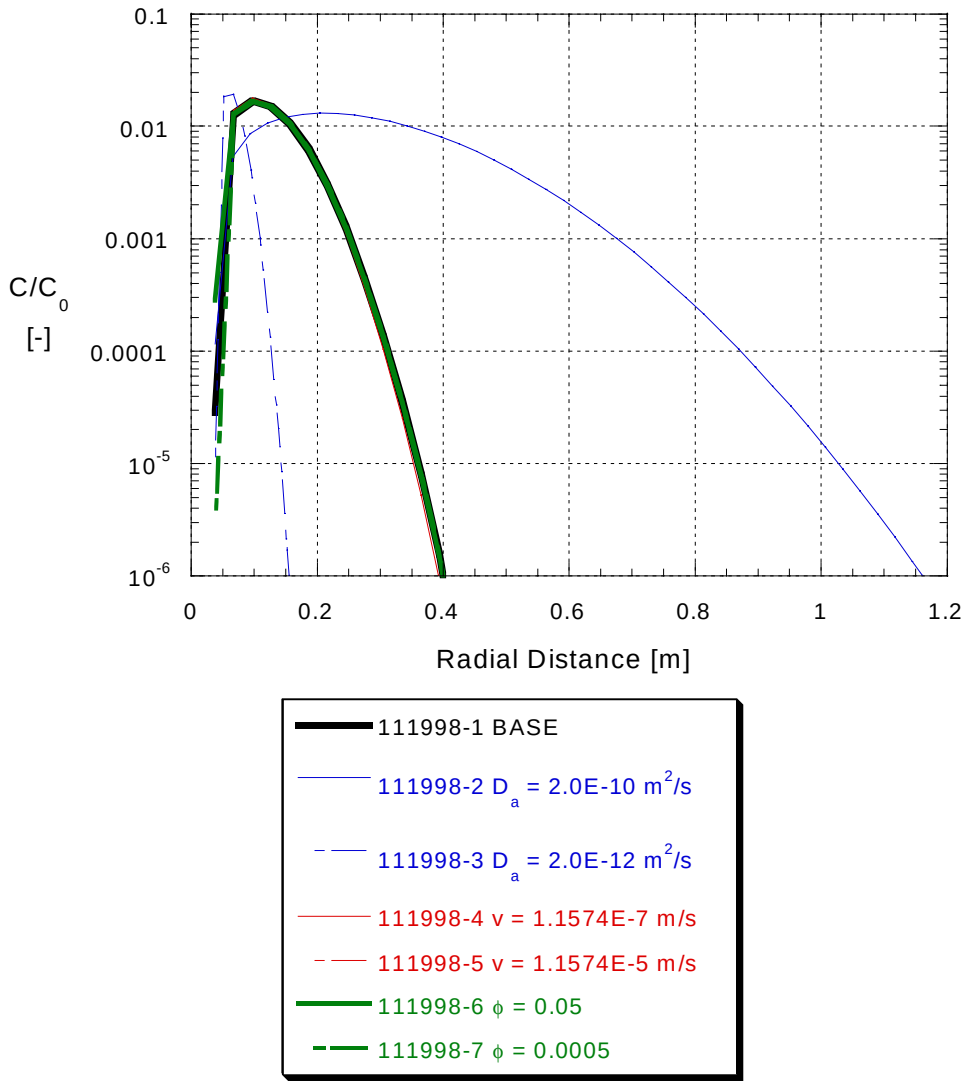

Figure 4-7. *Concentration profile at 5 years, case of rock with homogeneous diffusivity.*

Concentration profiles at 5 years are shown in Figure 4-7. Note that the concentrations shown in the profiles are concentration in the pore space – these concentrations presumably must be diluted either by rock or water in order to be measured. Again, we can see that for the Base Case the relative concentration drops to a very small fraction by a radial distance of 0.4 m.

4.2.3 Natural tracer experiments, heterogeneous rock

Scoping calculations were conducted to investigate the influence of heterogeneity in apparent diffusivity on the experiment with a natural tracer. The model used to describe this heterogeneity is similar to that of Haggerty and Gorelick /1998/ and Haggerty et al, 1998 /in revision/, where the apparent diffusivity is characterized by a lognormal distribution. The rock is assumed comprised of a network of diffusion pathways, each of which has a different value of D_a. Although in this work we assume mathematically that the

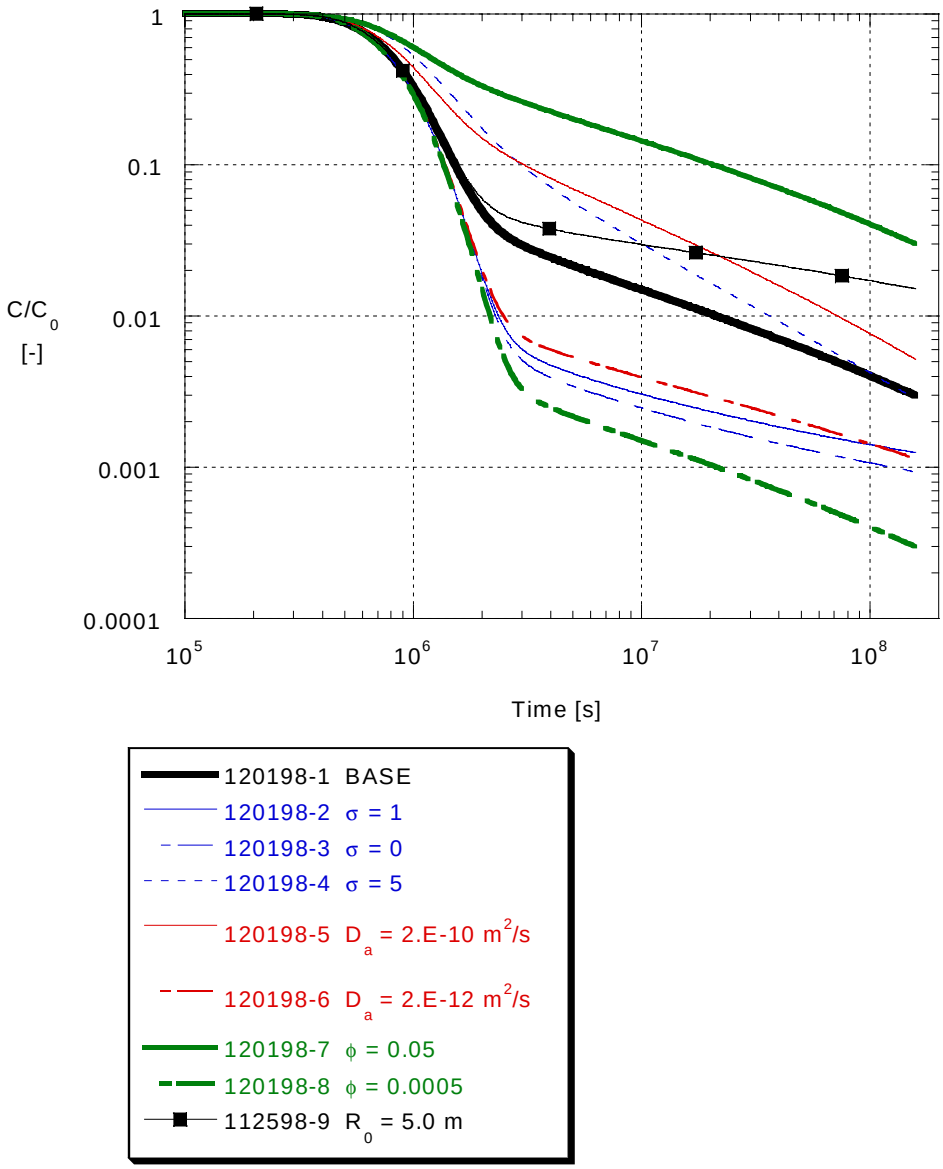

Figure 4-8. *Concentration histories for a natural tracer in rock with heterogeneous diffusivity.*

pathways are of the same lengths (0.50 m), for the situation we are modeling the variability in D_a is equivalent to variability in $1/l^2$, and therefore such variability is implicitly accounted for. The parameters of the lognormal distribution are the geometric mean of the diffusivity, which we assume equal to 2.0 x 10^{-11} m^2/s, and the standard deviation of the logarithm of D_a, σ. Keeping in mind that we are implicitly accounting for both variability in D_a and variability in the length of the diffusion pathway, we set σ equal to 3 for the Base Case. Similar and larger values for σ have been found by Pedit and Miller /1994/, Werth et al /1997/, Haggerty and Gorelick /1998/, and others. Also note that, based on the discussion in Section 3.3, larger values may be justifiable at Äspö and elsewhere in Fenno-Scandian granitic rocks.

Key results for the scoping calculations on the natural tracer in heterogeneous rock are shown in Figure 4-8. The primary effect of heterogeneity in D_a is in the late-time slope of the concentration histories. Comparing the late-time behavior for σ = 0, 3 (Base

Case), and 5, we see progressively lower slopes. This is similar to the effects of heterogeneity in diffusivities that we see in other types of tests (i.e., column tests, Haggerty and Gorelick /1998/, and single-well injection-withdrawal tests, Haggerty et al, 1998 /in revision/). For this reason, it appears that it may be possible to distinguish homogeneous and heterogeneous diffusion in a LTDE with a natural tracer.

At this point it is important to raise a concern over the possibility of misinterpreting the results of heterogeneous diffusion as homogeneous diffusion with a larger apparent diffusivity. From Figure 4-8 we can see that the late-time behavior of the heterogeneous D_a concentration histories could lead to very poor estimates of diffusivity if the wrong model of diffusion (i.e., homogeneous diffusion) were applied. Application of a homogeneous model of diffusion to the Base Case ($\sigma = 3$, i.e., significantly heterogeneous diffusion) would lead to a serious overestimation of diffusivity. The reason for this is that larger values of σ lead to late-time concentrations that are larger. The only way to get such larger late-time concentrations with a homogeneous model is to either (a) assume larger-than-correct porosity or (b) assume larger-than-correct diffusivity. Since porosity is relatively well-known, the error would almost certainly be to assume diffusivity is larger. Such an overestimate applied to the Performance Assessment would ultimately lead to underestimates of radionuclide transport velocity away from a repository.

4.2.4 Injected tracer experiments, heterogeneous rock

Lastly, scoping calculations were performed assuming heterogeneous diffusion with the injected tracer experiments. The Base Case simulation was identical to that for the natural tracer except that the tracer was injected into the central well for 0.5 yr, then the well was flushed with tracer-free water for another 4.5 yr.

Key results from these scoping calculations are shown in Figure 4-9. The main influence of heterogeneous diffusivity is to raise the late-time concentrations above what they would be if diffusivity were homogeneous. Larger values of σ (i.e., $\sigma = 3$ or 5) result in late-time concentrations that are significantly larger than for homogeneous diffusivity. There is also a subtle late-time effect on the slope of the concentration history. Overall, the injected tracer test experiments are not expected to be as helpful as the natural tracer experiments in evaluating heterogeneity in diffusivity. Ultimately the reason for this lies in the fact that the injected tracers are only injected for 0.5 years – the tracer test would be better at distinguishing heterogeneity if they could be injected for a significantly longer time.

Note, however, that other than the magnitude of the concentrations, the concentration history of the injected tracer test is insensitive to heterogeneity in diffusivity. The late-time slope, the key signature of heterogeneous diffusivity in the work of Haggerty and Gorelick /1998/ and Haggerty et al, 1998 /in revision/, is not noticeably different from the case of homogeneous diffusivity. As a result it is apparent that the injected tracer tests may not be useful in characterizing heterogeneity in diffusivity.

The same concern raised in the discussion of the natural tracer test must be raised for the injected tracer – the risk of misinterpretation of LTDE data. The fundamental problem of heterogeneous diffusivity occurs when the data are interpreted using a homogeneous model. In the scoping calculations shown in Figure 4-9, heterogeneous diffusivity increases the observed late-time concentration. If interpreted with a model

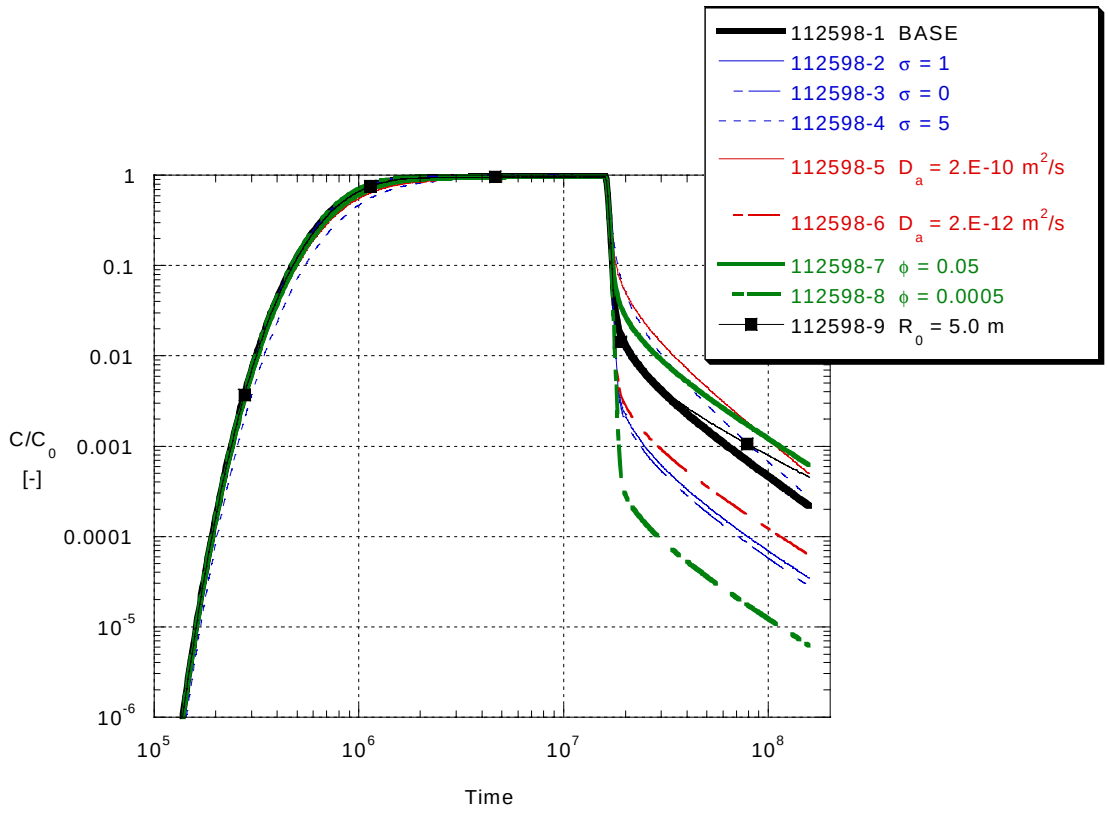

Figure 4-9. *Concentration histories for injected tracer in rock with heterogeneous diffusivities.*

assuming homogeneous diffusivity, the resulting estimate of apparent diffusivity will be larger than the true mean apparent diffusivity. Presumably, this larger apparent diffusivity would be applied to the entire volume of rock in the context of Performance Assessment calculations. The result would be that the entire volume of rock is assigned an apparent diffusivity that is larger than the true mean diffusivity. As a consequence, a radionuclide would be modeled as having a much larger apparent retardation factor than is, in fact, the case. The ultimate result could be a non-conservative model of radionuclide release to the environment.

5 Development of advection-anomalous diffusion model

One of the goals of the project was to work toward development of an advection-dispersion model coupled to anomalous diffusion. As stated in the testplan, we expected that we would only be able to make some small steps toward development of such a model. This turned out to be an accurate prediction, although we made more progress than we had originally thought we might. This small section describes a mathematical technique that should prove adequate for building such a model and some results from our first attempt at its construction.

We modeled transport with anomalous diffusion using a modified form of Giona et al's /1996a/ input/output renormalization method for diffusion on fractals. We very briefly outline the major steps of this analysis. First, the diffusion equation is written in finite difference form so as to be usable on a discrete fractal lattice:

$$\frac{\partial c_i}{\partial t} = \frac{D_a}{\Delta x^2}\left[\sum_{j=1}^{N} H_{ij}c_j - pc_i + \delta_{i1}\left(c_b - c_1\right)\right] \tag{5-1}$$

where c is concentration and the subscript indicates the location in the lattice; Δx is the lattice spacing; H_{ij} is the adjacency matrix (nodes i and j are adjacent and connected if H_{ij} is 1, and unconnected if H_{ij} is 0); p is the coordination number sites; and δ_{i1} is a Kronecker delta which is only nonzero if $i = 1$. Note that c_b is the boundary concentration, and will generally be an unknown function of time; it will be determined by coupling this system of equations with the advective-dispersive PDE. Also note that (5-1) is easily modified to allow variable D_a , if desired.

Equation (5-1) is simplified by temporarily neglecting one of the boundary terms (the term is added back later by a second renormalization). The equation is then converted to the Laplace domain and rearranged, resulting in the following solution:

$$\bar{\boldsymbol{c}} = \frac{D_a}{\Delta x^2}\left[\left(s + p\frac{D_a}{\Delta x^2}\right)\boldsymbol{I} - \boldsymbol{H}\right]^{-1}\bar{c}_0\boldsymbol{e_1} \tag{5-2}$$

where bold-face indicates a vector or matrix; the overbar indicates a Laplace-domain function; s is the Laplace parameter; $\boldsymbol{I}$ is the identity matrix; $\boldsymbol{H}$ is the adjacency matrix; and $\boldsymbol{e}_1$ is $(1,0,....,0)^t$. Equation (5-2) could be used to solve a number of fractal diffusion problems directly, except that the matrix inversion makes the solution infeasible as written (a typical matrix could be 10^9 x 10^9 or larger for a 3-D problem). Giona et al /1996a/ follow the work of Schwalm and Schwalm /1988/ and resort to Green function analysis, where the Green function in (5-2) is

$$\overline{\boldsymbol{G}(z)} = \left[\left(s + p\frac{D_a}{\Delta x^2}\right)\boldsymbol{I} - \boldsymbol{H}\right]^{-1} = \left[z\boldsymbol{I} - \boldsymbol{H}\right]^{-1} \tag{5-3}$$

Note that only the first column of $\overline{\boldsymbol{G}(z)}$ is needed since only the first element of the column vector $\boldsymbol{e}_1$ is non-zero. The entire Green function can be found using the implicit recursive relationship:

$$\overline{\boldsymbol{G}^{(n+1)}} = \overline{\boldsymbol{G}^{*(n)}} + \overline{\boldsymbol{G}^{*(n)}}\boldsymbol{V}^{(n)}\overline{\boldsymbol{G}^{(n+1)}} \tag{5-4}$$

where all matrices but $\boldsymbol{V}^{(n)}$ are a function of z; $\overline{\boldsymbol{G}^{*(n)}}$ is the block-diagonal matrix whose blocks are equal to $\overline{\boldsymbol{G}^{(n)}}$; and $\boldsymbol{V}^{(n)}$ is a sparse matrix that contains the edges connecting the copies of the previous generation fractal together. Since only the first column of $\overline{\boldsymbol{G}(z)}$ is required, the recursion relationship can be simplified further, and can usually be reduced to a small number of algebraic equations. The particular algebraic equations depend on the fractal geometry. After these renormalization equations are found, it is necessary to do one further renormalization to include the boundary condition that was temporarily neglected prior to equation (5-2). Once this is completed, equation (5-2) may be solved for the desired boundary concentrations without the need for a large matrix inversion.

Preliminary Simulations: At this point we have solved the problem of advection and dispersion along a column in the presence of diffusion into and out of fractal grains for only one particular case. The fractal geometry we chose, for the purpose of an example, is a 50^{th}-generation, 3-D Sierpinski gasket. The algebraic recursion equations resulting from (5-4) are solved simultaneously with the advective-dispersive equation in the Laplace domain. Using the renormalization technique the problem runs in 10-20 seconds on a 200 MHz Pentium II (solution of an equivalent problem using finite differences/elements would require a 10^{30} x 10^{30} matrix and would be infeasible even on a supercomputer).

Figure 5-1 shows breakthrough curves (BTC) for a Dirac injection into a column 30 cm long with a pore-fluid velocity of 0.1 cm/s and a dispersivity of 0.3 cm. The grain size is 0.5 cm. BTCs are shown for the scale invariant matrix (anomalous diffusion), a multi-rate matrix (lognormal distribution of diffusion rate coefficients, with a log standard deviation of 3) and conventional diffusion into spherical grains (diffusion in a homo-geneous matrix). The slowest long-term recovery is from the scale invariant matrix, while the scale invariant matrix also has the earliest breakthrough and highest peak concentration in the breakthrough curve.

Anomalous diffusion (diffusion into the scale invariant matrix), multirate diffusion, and conventional diffusion into a homogeneous matrix are distinguishable by the shapes of the tails of the BTC. The tail of the conventional BTC is goes asymptotically to an infinite slope, while both multirate and anomalous diffusion have near-constant late-time slopes (this can be shown analytically). At intermediate times, the conventional BTC goes has a power-law behavior of $t^{-3/2}$ (note that in the case of an infinite block, the conventional BTC also goes as $t^{-3/2}$ at late time /e.g., Hadermann and Heer, 1996; also see Section 6.2.1/). The late-time BTC for the scale invariant matrix goes as $t^{-2+d_s/2}$, which gives a slope of approximately -1.2 for a 3-D Sierpinski gasket. The late-time BTC slope for the multirate matrix is approximately -2.5 for a lognormal distribution and large standard deviation (steeper for smaller standard deviations). Note, however, that at very late time the multirate lognormal matrix would have an infinite slope.

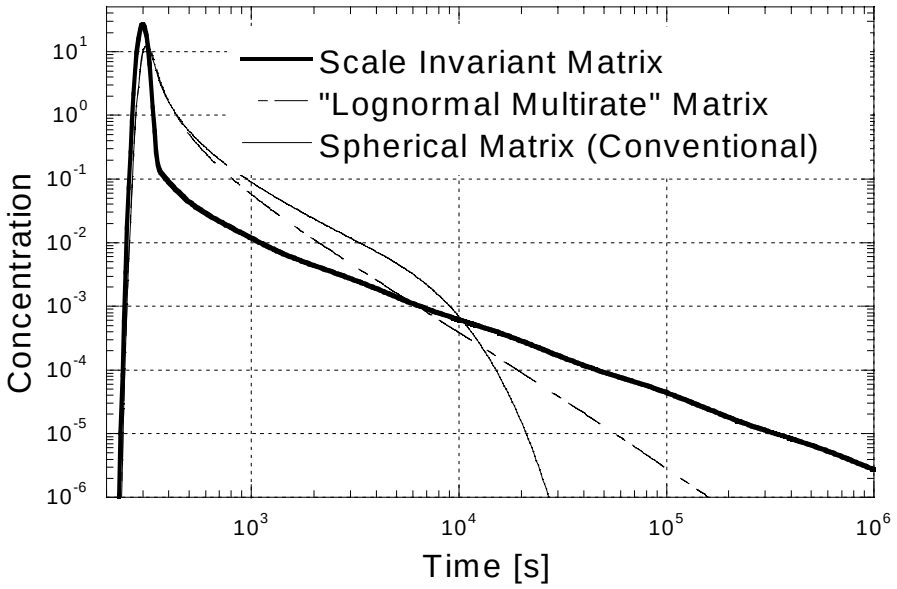

Figure 5-1. *Breakthrough curves (BTC) for advective-dispersive transport in the presence of diffusion within a scale invariant matrix, a multirate matrix, and a conventional spherical matrix. Note the true power-law behavior of the scale-invariant matrix, and the approximate power-law behavior of the lognormal multirate matrix.*

6 Investigation of late-time behavior of breakthrough curves and their significance

The purpose of this section is to explore the nature of tailing in tracer test breakthrough curves (BTCs). We will focus on understanding (1) the late-time slope of BTCs for a range of mass transfer models; (2) what information can be provided by the late-time behavior of the BTC; and (3) what models of mass transfer provide power-law BTCs at late time. Expressions describing the late-time BTCs for single-rate models with both infinite and finite immobile zones, as well as multirate models with first-order and diffusion rate coefficients defined by lognormal, gamma and power-law distributions are derived. Implications of the late-time slopes defined by these equations are discussed with respect to mass transfer processes.

An area of particular interest in this section is power-law behavior at late time in BTCs. Power-law behavior in BTCs ($c \sim t^{-k}$) has been noted in a number of laboratory and field experiments. Farrell and Reinhard /1994/ and Werth et al /1997/ obtained power-law BTC and mass recovery curves with sorbing organic solutes in unsaturated media. Cunningham et al /1997/ were able to represent the Werth et al /1997/ data with a gamma distribution of diffusion rate coefficients, while Haggerty and Gorelick /1998/ were able to approximate the power-law behavior with a lognormal distribution of diffusion rate coefficients. Both Cunningham et al /1997/ and Haggerty and Gorelick /1998/ noted the inability of conventional models of mass transfer to yield the appropriate power-law behavior. Power-law behavior with $k = 3/2$ has been observed in field data from the Grimsel test site and has been adequately explained with conventional (single-rate) diffusion /Eikenberg et al, 1994; Hadermann and Heer, 1996/. However, single-rate diffusion is only able to yield a power-law of exactly $t^{-3/2}$, and can only maintain this behavior slightly longer than the mean immobile-zone residence time ($t_\alpha = a^2/15D_a$ for spheres and $a^2/15D_a$ for layers), where D_a is the apparent diffusivity and a is the half-thickness of the immobile zone. Power-law behavior such as that observed in Farrell and Reinhard /1994/, Werth et al /1997/, or Meigs and Beauheim /in review/ cannot be explained with conventional single-rate diffusion.

As we will see in this section, power-law behavior at late time is particularly significant for mass transfer. In particular, if the power is small (less than 3), it suggests at a minimum that the mean time-scale of mass transfer is longer than the experiment and possibly that the mean time-scale is infinite (undefined). Such a power-law behavior may be indicative of a fractal pore geometry and anomalous diffusion, though such a conclusion remains tentative at this point.

6.1 Mathematical development

6.1.1 General case

Late-time solution for concentration:

The mass balance equation for a solute advecting and dispersing in 1-D, and interacting with rock via equilibrium sorption plus diffusion and/or linear nonequilibrium sorption is:

$$\frac{\partial}{\partial x}\left(\frac{\alpha_L v}{R_a}\frac{\partial c}{\partial x} - \frac{v}{R_a}c\right) = \frac{\partial c}{\partial t} + \Gamma(t) \tag{6-1}$$

where α_L [L] is longitudinal dispersivity; v [LT^{-1}] is pore-fluid velocity; R_a [-] is the retardation factor in the advective (effective or kinematic) porosity; c [ML^{-3}] is solute concentration within the advective porosity; and $\Gamma(t)$ is the source-sink term for mass exchange with the diffusive (matrix) porosity and nonequilibrium sorption sites. We will employ the uniform initial conditions

$$c(x,\, t = 0) = c_m(x,\, z,\, t = 0) = c_0 \tag{6-2}$$

where c_m [ML^{-3}] is solute concentration within the matrix porosity (immobile domain), which may be a function of a second spatial coordinate z. We will also employ the boundary conditions

$$c(x{=}0,\, t) = m_0\delta(t) \tag{6-3}$$

$$c(x \to \infty,\, t) = c_0 \tag{6-4}$$

where m_0 [MTL^{-3}] is the zeroth moment of the concentration history and $\delta(t)$ is the Dirac delta [T^{-1}].

If input concentration is changed (e.g., pulse or Dirac injection), then at late time:

$$\alpha_L\frac{\partial c}{\partial x} << c\,, \quad t >> t_{ad} \tag{6-5}$$

where t_{ad} is the average advective residence time (equal to xR_a/v if velocity is constant in space). In other words, once the input pulse has advected far past the point of observation x, then dispersion has a negligible effect on concentration. In the same way, if the immobile zone has an long average residence time relative to advection, then at late time:

$$\frac{\partial c}{\partial t} << \Gamma(t), \quad t >> t_{ad} \text{ and } t_\alpha >> t_{ad} \tag{6-6}$$

where t_α is the average residence time in the immobile zone. In other words, concentration change at late time is dominated by exchange between the mobile and immobile zones if the average immobile zone residence time is longer than the advective time. Note that from this point forward, it will be assumed that $t_\alpha >> t_{ad}$ and $t >> t_{ad}$ unless otherwise stated. Therefore the equation (6-1) may be re-written:

$$-\frac{\partial}{\partial x}\left(\frac{v}{R_a}c\right) = \Gamma(t) \tag{6-7}$$

By integration we can obtain a solution for concentration at late time:

$$c = -\int_0^L \frac{R_a}{v}\Gamma(t)dx \tag{6-8}$$

This function is correct even if $\Gamma(t)$ is spatially variable. As we will see shortly, $\Gamma(t)$ can be removed from the integral if the coefficients contained in $\Gamma(t)$ are spatially uniform. Therefore, this leaves us with a very simple expression for concentration at late time:

$$c = -t_{ad}\Gamma(t) \tag{6-9}$$

Source-sink term Γ(t):

For any linear mass transfer problem with uniform initial conditions it is possible to express the source-sink term as /modified from Carrera et al, 1998/:

$$\Gamma(t) = \int_0^t \frac{\partial c(t-\tau)}{\partial t} g(\tau)d\tau = \frac{\partial c}{\partial t} * g = c * \frac{\partial g}{\partial t} + cg_0 - c_0 g \tag{6-10}$$

where $g(t)$ is a "memory function"; * represents convolution product; g_0 is the memory function at $t = 0$ and c_0 is the initial concentration. The last transformation in (6-10) is most easily derived in the Laplace domain. The memory function $g(t)$ may be physically interpreted as β_{tot} times residence time distribution in the immobile zone given a unit impulse at the surface. The derivative of $g(t)$ is proportional to what is commonly called in statistical physics the probability of first return or distribution of first passage times /e.g., Bouchaud and Georges, 1990, p. 271–272/. The coefficient β_{tot} is the capacity coefficient (see Section 6.3.1) and is the ratio of mass in the matrix to mass in the mobile domain at equilibrium.

We recognize that the concentration is well approximated by the boundary condition $m_0\delta(t)$ for the following conditions: (1) at late time; and (2) calculation of the source-sink term which only requires an approximation of the mobile-domain concentration for use in calculating a concentration gradient. Therefore, (6-10) can be expressed:

$$\Gamma(t) \cong m_0 \frac{\partial g}{\partial t} - c_0 g \ , \quad t >> t_{ad} \ \text{ and } \ t_\alpha >> t_{ad} \tag{6-11}$$

We see from (6-9) and (6-11) how the memory function may be interpreted physically. The memory function is proportional to the late-time concentration from a purge experiment /e.g,. Farrell and Reinhard, 1994; Werth et al, 1997/ where the medium begins the experiment with a uniform concentration of tracer and is flushed by a tracer-free solution.

The general form of the memory function is /modified from Carrera et al, 1998/

$$g(t) = \int_0^\infty \alpha b(\alpha)\, e^{-\alpha t} d\alpha \tag{6-12}$$

where α is a rate coefficient and $b(\alpha)$ is a density function of rate coefficients. Note two differences between our definition of the memory function and that of Carrera et al /1998/. First, our $g(t)$ includes the constants that are placed before the source-sink term in Carrera et al's mass balance equation. Secondly, although Carrera et al /1998/ express (6-12) as a discrete function, the more general expression is as a continuous function, allowing for density functions of diffusion rate coefficients, etc. Various distributions of $b(\alpha)$ are given in Table 6-1, along with the corresponding function $g(t)$.

We note that (6-12) is the Laplace transform of $\alpha\, b(\alpha)$. where t is treated as the Laplace variable. We also use the property of the Laplace transform /e.g., Roberts and Kaufman, 1966/

$$\text{Lap}\left\{\alpha^2 b(\alpha)\right\} = \frac{\partial g}{\partial t} \tag{6-13}$$

where Lap{*} indicates the Laplace transform.

Employing (6-9), (6-11), (6-12), and (6-13), we can now write an approximation for concentration at late time:

$$\begin{aligned} c &= t_{ad}\left(c_0 g - m_0 \frac{\partial g}{\partial t}\right) \\ &= t_{ad} \int_0^\infty \left(c_0 + \alpha m_0\right) \alpha b(\alpha)\, e^{-\alpha t} d\alpha \\ &= t_{ad}\, \text{Lap}\left\{\left(c_0 + \alpha m_0\right) \alpha b(\alpha)\right\} \end{aligned} \tag{6-14}$$

All forms of (6-14) are equivalent and are useful in different ways for understanding the late-time behavior of BTCs. We expect that in most applications only one of c_0 or m_0 will be non-zero; however, (6-14) holds true regardless of the values of c_0 and m_0.

Table 6-1. Density functions $b(\alpha)$, corresponding memory functions $g(t)$, and corresponding harmonic mean rate coefficient α_H.

Model	$b(\alpha)$	$g(t)$	$\hat{\alpha}_H$
First-order	$\beta_{tot}\delta(\alpha-\alpha^*)$	$\alpha^*\beta_{tot}e^{-\alpha^* t}$	α^*
Multirate	$b(\alpha)$	$\int_0^\infty \alpha b(\alpha)e^{-\alpha t}d\alpha$	$\beta_{tot}\left(\int_0^\infty \frac{b(\alpha)}{\alpha}d\alpha\right)^{-1}$
Gamma distribution	$\frac{\beta_{tot}}{\gamma^\eta\Gamma(\eta)}\alpha^{\eta-1}e^{-\alpha/\gamma}$	$\beta_{tot}\gamma\eta\,(\gamma t+1)^{-\eta-1}$	$0 \quad ,\eta\le 1$ $(\eta-1)\gamma \quad ,\eta>1$
Power-law distribution*	$\sim \alpha^{k-3}$	$\sim t^{1-k}$	$0 \quad ,k\le 3$ $\frac{(k-3)}{(k-2)}\alpha_{\max} \quad ,k>3$
Diffusion: Finite layer	$\sum_{j=1}^{\infty}\frac{8\beta_{tot}}{(2j-1)^2\pi^2}\delta_j\left[\alpha-\frac{(2j-1)^2\pi^2}{4}\frac{D_a}{a^2}\right]$	$\sum_{j=1}^{\infty}2\beta_{tot}\frac{D_a}{a^2}\exp\left[-\frac{(2j-1)^2\pi^2}{4}\frac{D_a}{a^2}t\right]$	$3\frac{D_a}{a^2}$
Diffusion: Infinite layer**	$\lim_{a\to\infty}\sum_{j=1}^{\infty}\frac{8R_{im}\theta_{im}a_w a}{(2j-1)^2\pi^2 R_m}\delta_j\left[\alpha-\frac{(2j-1)^2\pi^2}{4}\frac{D_a}{a^2}\right]$	$\frac{\theta_{im}R_{im}a_w}{R_m}\sqrt{\frac{D_a}{\pi t}}$	0

* See Section 6.2.4 for details. Note that the harmonic mean is given assuming that $\alpha_{min} = 0$.

** Where R_{im} [-] is matrix retardation factor; θ_{im} [-] is matrix porosity; a_w [L^{-1}] is the specific surface area of matrix.

To be contd.

Table 6-1 (contd.)

Diffusion: Cylinder***	$\sum_{j=1}^{\infty} \frac{4\beta_{tot}}{u_j^2} \delta_j \left[\alpha - u_j^2 \frac{D_a}{a^2}\right]$	$\sum_{j=1}^{\infty} 4\beta_{tot} \frac{D_a}{a^2} \exp\left[-u_j^2 \frac{D_a}{a^2} t\right]$	$8 \frac{D_a}{a^2}$
Diffusion: Sphere	$\sum_{j=1}^{\infty} \frac{6\beta_{tot}}{j^2\pi^2} \delta_j \left[\alpha - j^2\pi^2 \frac{D_a}{a^2}\right]$	$\sum_{j=1}^{\infty} 6\beta_{tot} \frac{D_a}{a^2} \exp\left[-j^2\pi^2 \frac{D_a}{a^2} t\right]$	$15 \frac{D_a}{a^2}$
Diffusion: Lognormal D_a/a^2 ****	$\sum_{j=1}^{\infty} \frac{8\beta_{tot}}{\sqrt{2\pi^5}(2j-1)^2 \sigma \alpha} \exp\left(-\frac{\left\{\ln\left[\frac{4\alpha}{(2j-1)^2\pi^2}\right] - \mu\right\}^2}{2\sigma^2}\right)$	Must be obtained numerically	$3 \exp\left(\mu - \frac{\sigma^2}{2}\right)$
Diffusion: Gamma D_a/a^2 ****	$\sum_{j=1}^{\infty} \frac{8\beta_{tot}}{(2j-1)^2\pi^2\Gamma(\eta)\alpha} \left[\frac{4\alpha}{\gamma(2j-1)^2\pi^2}\right]^{\eta} \exp\left[-\frac{4\alpha}{\gamma(2j-1)^2\pi^2}\right]$	$\sum_{n=1}^{\infty} 2\beta_{tot}\gamma\eta \left[\gamma t \frac{(2j-1)^2\pi^2}{4} + 1\right]^{-\eta-1}$	$0 \quad , \eta \le 1$ $3(\eta-1)\gamma \quad , \eta > 1$

*** Where u_j is the j^{th} solution of $J_0(u_j) = 0$, where J_0 is a Bessel function of the first kind.

**** This is a distribution of 1-dimensional pathways or layers.

6.1.2 Notes on application of equation (6-14)

Equation (6-14) presents an interesting theoretical development for two reasons. First, the late-time behavior of the BTC is easily obtained for a wide variety of density functions $b(\alpha)$ using any comprehensive table of Laplace transforms.

Second, (6-14) suggests that the distribution of mass transfer rate coefficients (whether from diffusion, nonequilibrium sorption, or a general distribution of mass transfer processes) is available directly and analytically from breakthrough data. In fact, if (6-14) is treated as an integral equation where $b(\alpha)$ is an unknown, the distribution $b(\alpha)$ may be directly calculated using the inverse Laplace transform. If the medium is initially free of tracer, then $c_0 = 0$ and the density function $b(\alpha)$ is given analytically by:

$$b(\alpha) = \frac{1}{t_{ad} m_0 \alpha^2 (2\pi i)} \int_{h-i\infty}^{h+i\infty} c(x= L,\, t)\, e^{-\alpha t} dt = \frac{1}{t_{ad} m_0 \alpha^2} \mathrm{Lap}^{-1}\left\{ c(x= L,\, t) \right\} \qquad (6\text{-}15)$$

A similar equation may be easily constructed for the case of non-zero initial conditions and continuous flushing of tracer-free fluid, such as in a purge experiment. Unfortunately, the practical use of (6-15) is limited by the conditions that we can only use the late-time breakthrough data, and that any errors in the data introduce numerical instabilities in the inverse Laplace transform. Nonetheless, (6-15) will allow us to determine certain important properties of the density function $b(\alpha)$.

6.1.3 Notes on the density function *b*(α)

We add two notes regarding the density function $b(\alpha)$ before continuing. First, a useful definition is that of the 0^{th} moment of the distribution of rate coefficients:

$$\int_0^\infty b(\alpha) d\alpha = \beta_{tot} \qquad (6\text{-}16)$$

where β_{tot} is commonly known as the capacity coefficient. The capacity coefficient is the ratio of mass in the immobile domain to mass in the mobile domain at equilibrium; in the absence of sorption it is the ratio of the two volumes.

Second, we note without derivation that the Laplace transform of the normalized distribution of rate coefficients is a particularly useful function by itself. This function is proportional to the mass fraction remaining in a matrix, where the initial conditions are uniform concentration in the matrix and the boundary condition of the matrix is zero concentration. The mass fraction remaining (M/M_0) is therefore:

$$\frac{M}{M_0} = \frac{\mathrm{Lap}\left\{ b(\alpha) \right\}}{1 + \beta_{tot}} = \frac{\int_0^\infty g(\tau)\, d\tau}{1 + \beta_{tot}} \qquad (6\text{-}17)$$

In other words, the mass fraction remaining is calculated simply by finding the Laplace transform of the distribution $b(\alpha)$.

6.1.4 Mean residence time

The residence time distribution in the immobile zone given a unit impulse at the surface is $g(t)/\beta_{tot}$. The mean residence time is therefore

$$\begin{aligned} t_\alpha &= \frac{1}{\beta_{tot}} \int_0^\infty t g(t) dt \\ &= \frac{1}{\beta_{tot}} \int_0^\infty t \int_0^\infty \alpha b(\alpha)\, e^{-\alpha t}\, d\alpha\, dt \\ &= \frac{1}{\beta_{tot}} \int_0^\infty \frac{b(\alpha)}{\alpha} d\alpha \end{aligned} \tag{6-18}$$

It can be shown /e.g., Cunningham and Roberts, 1998/ that the zeroth, first, and second temporal moments are the same for any distribution of rate coefficients provided that the mean residence time in the immobile zone is the same. Therefore, the best "effective" rate coefficient is the harmonic mean:

$$\hat{\alpha}_H = \frac{1}{t_\alpha} = \beta_{tot} \left(\int_0^\infty \frac{b(\alpha)}{\alpha} d\alpha \right)^{-1} \tag{6-19}$$

Notably, the harmonic mean may be zero for some distributions, meaning that the mean residence time in the immobile zone is infinity. The harmonic mean for a number of distributions $b(\alpha)$ is shown in Table 6-1. Note also that the harmonic mean rate coefficient for the conventional diffusion models (spheres, cylinders, and layers) is the same as that given by Glueckauf /1955/, Goltz and Roberts /1987/ and others.

6.2 Late-time behavior of BTCs

In this section we will consider a number of examples of BTCs after a pulse injection into a medium with zero initial concentration. Many of the functions developed in this section are summarized in Table 6-1, as well as several others not discussed here.

6.2.1 Simple case: Finite spherical blocks

Consider the case of finite spherical blocks. Haggerty and Gorelick /1995/ showed that a particular discrete distribution of first-order rate coefficients results in a model that is mathematically identical, from the perspective of the mobile domain concentrations, to that of diffusion into and out of various matrix geometries. In the case of spherical blocks, the distribution is

$$b(\alpha) = \sum_{j=1}^{\infty} \frac{6\beta_{tot}}{j^2\pi^2} \delta_j \left(\alpha - j^2\pi^2 \frac{D_a}{a^2} \right) \tag{6-20}$$

where β_{tot} [-] is the capacity coefficient of the spherical blocks; D_a [T^{-1}] is the apparent diffusivity; and a [L] is the radius of the spherical blocks. This distribution is a series of Dirac deltas with monotonically decreasing weight. The harmonic mean is the well-known linear driving force approximation 15 D_a/a^2 /e.g., Glueckauf, 1955/. The memory function is

$$g(t) = -\sum_{j=1}^{\infty} 6\beta_{tot}\frac{D_a}{a^2}\exp\left(-j^2\pi^2\frac{D_a}{a^2}t\right) \tag{6-21}$$

Readers familiar with diffusion in spherical geometry will recognize (6-21) as proportional to the mass flux out of spheres initially saturated with a uniform solute. mass fraction and with a boundary concentration of zero. /e.g., Crank, 1975; Grathwohl et al, 1994/.

The resulting late-time approximation for concentration in the mobile domain (with initial concentration of zero) is given by substituting (6-21) into (6-14):

$$c = m_0 t_{ad}\beta_{tot}\left(\frac{D_a}{a^2}\right)^2\sum_{j=1}^{\infty} 6j^2\pi^2\exp\left(-j^2\pi^2\frac{D_a}{a^2}t\right) \tag{6-22}$$

From this expression, we can see that the late-time concentration is proportional to $\exp(-\pi^2 D_a t/a^2)$; therefore, on a double-log plot, the late-time slope will approach $-\infty$ shortly after the mean residence time in the immobile zone ($t_\alpha = a^2/15D_a$) is reached.

Figure 6-1 shows the full solution to the advection-dispersion-mass transfer (ADMT) equations and the late-time approximation. The ADMT equations were solved using STAMMT-L /Haggerty and Reeves, 1999/ for m_o = 1 x 10^4 s kg m^{-3}; t_{ad} = 1 x 10^4 s; D_f/a^2 = 1 x 10^{-8} s^{-1}; β_{tot} = 1; and a Peclet number of 1000. All concentrations have been non-dimensionalized by the terms in front of the infinite series in (6-22).

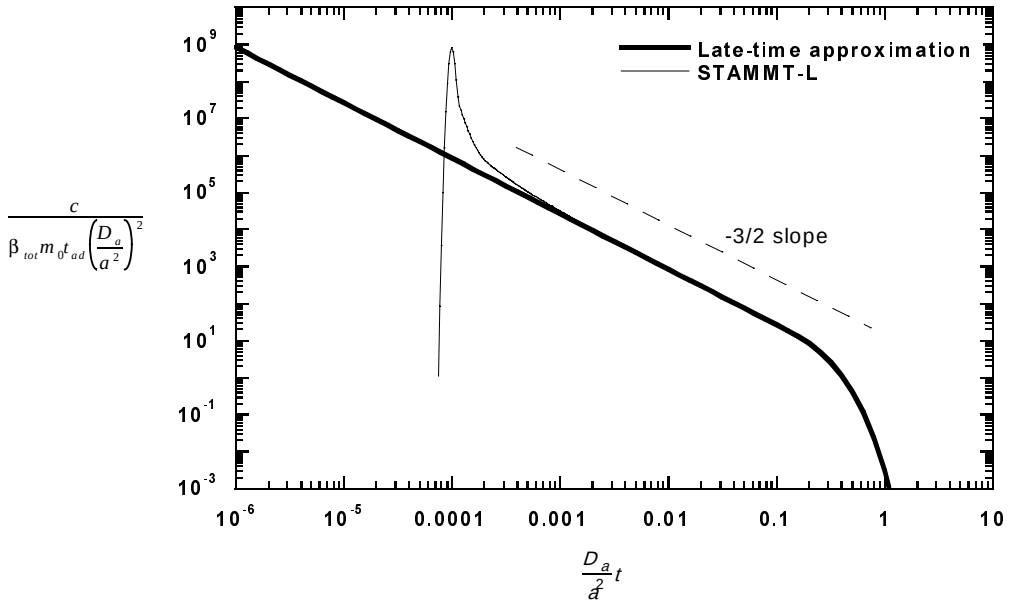

Figure 6-1. *Late-time approximation and full solution to advection-dispersion-mass transfer equations for spherical diffusion. The vertical axis is nondimensional concentration and the horizontal axis is nondimensional time (i.e., the Fourier number).*

From Figure 6-1 we make four points. First, the approximation does not contain the advective-dispersive peak, but does very accurately represent the late-time behavior of the of the ADMT equation. We can see in the figure that the late-time approximation is valid when $t >> t_{ad}$ provided that $t_\alpha >> t_{ad}$. Second, the late-time behavior contains the well-known -3/2 double-log slope for matrix diffusion, which ends when $tD_d/a^2 > 1$. In the case of infinitely large matrix blocks, the -3/2 behavior would continue indefinitely because tD_d/a^2 never reaches 1. Third, the location of the BTC peak in the ADMT solution will move back and forth on the late-time approximation curve, dependent on the relative values of t_{ad} and D_d/a^2. Last, we note that it is possible to estimate both β_{tot} and D_d/a^2 by using the late-time approximation as a type-curve. The capacity coefficient β_{tot} would be estimated from the vertical shift, while D_d/a^2 would be estimated from the horizontal shift.

6.2.2 Gamma distribution of first-order rate coefficients

Gamma distributions of rate coefficients have been used to represent multirate mass transfer in several papers. Cunningham et al, /1997/ developed the mathematics of a gamma distribution of diffusion rate coefficients, while Werth et al /1997/ applied this model successfully to several mass fraction remaining data sets. Connaughton et al, /1993/ used a gamma distribution of first-order rate coefficients to model release of naphthalene from soil, while Pedit and Miller /1994/ employed a gamma distribution of first-order rate coefficients to examine diuron sorption. The method we are using is applicable to both distributions, and the key relationships for both are given in Table 6-1. Although the early time behavior will differ for gamma distributions of first-order and diffusion rate coefficients, the late-time slope will be identical for the same value of η.

The gamma distribution of first-order rate coefficients is

$$b(\alpha) = \frac{\beta_{tot}}{\gamma^\eta \Gamma(\eta)} \alpha^{\eta-1} e^{-\alpha/\gamma} \tag{6-23}$$

Of particular importance for applications is that the harmonic mean of (6-23) is 0 if η is less than or equal to 1, a fact that is true for distributions of either first-order rate coefficients or diffusion rate coefficients. As a consequence, the mean residence time in the immobile zone would be infinite.

The memory function is

$$g(t) = -\beta_{tot} \frac{\partial}{\partial t} (\gamma t + 1)^{-\eta} \tag{6-24}$$

Therefore, the late-time concentration in the fracture is given by

$$c = m_0 t_{ad} \beta_{tot} \gamma^2 \frac{\eta(\eta+1)}{(\gamma t + 1)^{\eta+2}} \tag{6-25}$$

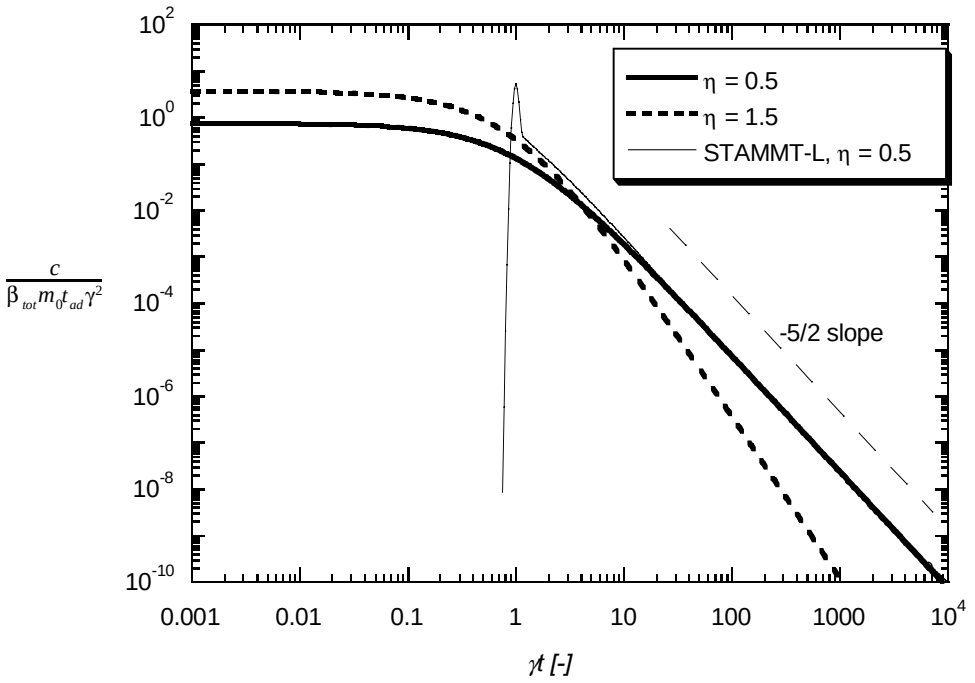

Figure 6-2. *Late-time solution and full ADMT solution for a gamma distribution of first-order rate coefficients.*

Note that at when $\gamma t >> 1$ the BTC follows a power-law:

$$c \sim t^{-\eta-2} \tag{6-26}$$

The same late-time power-law behavior is also exhibited with a distribution of diffusion rate coefficients. Note that a power-law behavior ($c \sim t^{-k}$) with $k < 3$ would indicate an infinite second (and higher) temporal moment and an infinite mean residence time in the immobile zone.

Figure 6-2 shows the late-time approximation in (6-25) nondimensionalized by the transport terms. We have normalized time by the characteristic mass transfer rate γ. Figure 6-2 also shows a solution to the ADMT equations with STAMMT-L (Haggerty and Reeves, 1999) for m_o = 1 x 10^4 s kg m^{-3}; t_{ad} = 1 x 10^4 s; γ= 1 x 10^{-4} s^{-1}; η = 0.5; β_{tot} = 1; and a Peclet number of 1000.

We see from (6-26) and Figure 6-14 that the late-time double-log slope of concentration will be -(η+2). For comparison to published values, Connaughton et al /1993/ estimated values of η in the range of 0.17 to 0.37 for a gamma distribution of first-order rate coefficients, while Pedit and Miller /1994/ estimated η = 0.11 from their experiments. Werth et al /1997/ found values of η equal to approximately 0.5 for a gamma distribution of diffusion rate coefficients. Note that all of these estimated η will lead to an infinite mean residence time within the immobile zone. Consequently, the variance of the breakthrough times will be infinite with these models.

6.2.3 Lognormal distribution of diffusion rate coefficients

Lognormal distributions of rate coefficients have also been used to represent mass transfer in natural systems. Pedit and Miller /1994/, Haggerty /1995/, and Culver et al /1997/, all used a lognormal distribution first-order rate coefficients to model uptake and release of sorbing solutes in soils. Pedit and Miller /1995/ and Haggerty and Gorelick /1998/ used a lognormal distribution of diffusion rate coefficients to model diffusion of sorbing solutes in soils. As is true for the gamma distributions of rate coefficients, the behavior of both lognormal models is very similar, especially at late time and large variances. In our analysis here we will employ only a distribution of diffusion rate coefficients:

$$b^*\left(\frac{D_a}{a^2}\right) = \frac{\beta_{tot}}{\sqrt{2\pi}\sigma\frac{D_a}{a^2}}\exp\left\{-\frac{\left[\ln\left(\frac{D_a}{a^2}\right)-\mu\right]^2}{2\sigma^2}\right\} \tag{6-27}$$

The equivalent distribution of first-order rate coefficients is given by Haggerty and Gorelick /1998/:

$$b(\alpha) = \sum_{j=1}^{\infty}\frac{8\beta_{tot}}{\sqrt{2\pi^5}(2j-1)^2\sigma\alpha}\exp\left(-\frac{\left\{\ln\left[\frac{4\alpha}{(2j-1)^2\pi^2}\right]-\mu\right\}^2}{2\sigma^2}\right) \tag{6-28}$$

The effective rate coefficient is 3 $\exp(\mu-\sigma^2/2)$. Consequently, the effective rate coefficient is approximately $0.22\sigma^2$ orders of magnitude smaller than the geometric mean. For large σ, the effective rate coefficient is approximately zero and the mean residence time in the immobile zone approaches infinity. In the limit of very large s, the distribution is log-uniform and is equivalent to a power-law distribution with $\sim\alpha^{-1}$. As we shall see in the following sections, this corresponds to a late-time BTC of $\sim t^{-2}$.

The Laplace transform of (6-28) must be done numerically. The result may then be inserted into (6-14). After taking the second derivative in time (numerically), the late-time approximation for a concentration BTC is shown in Figure 6-3 for various values of σ. The time axis of Figure 6-3 is normalized by the geometric mean of (6-23), and concentration is normalized the same as previously. Figure 6-3 also shows the solution to the ADMT equations in the presence of a lognormal distribution of diffusion rate coefficients. The ADMT equations were solved using STAMMT-L /Haggerty and Reeves, 1999/ for $m_o = 1 \times 10^4$ s kg m^{-3}; $t_{ad} = 1 \times 10^4$ s; $e^{-\mu} = 1 \times 10^{-4}$ s^{-1}; $\sigma = 5$; $\beta_{tot} = 1$; and a Peclet number of 1000. The discrepancy at late time is due to numerical error in the series of numerical steps for the late-time approximation; however, the late-time slopes are correct. Note that the late-time slopes for the lognormal distribution lie between 2 and 3 for a large range of time, provided that σ is greater than approximately 3.

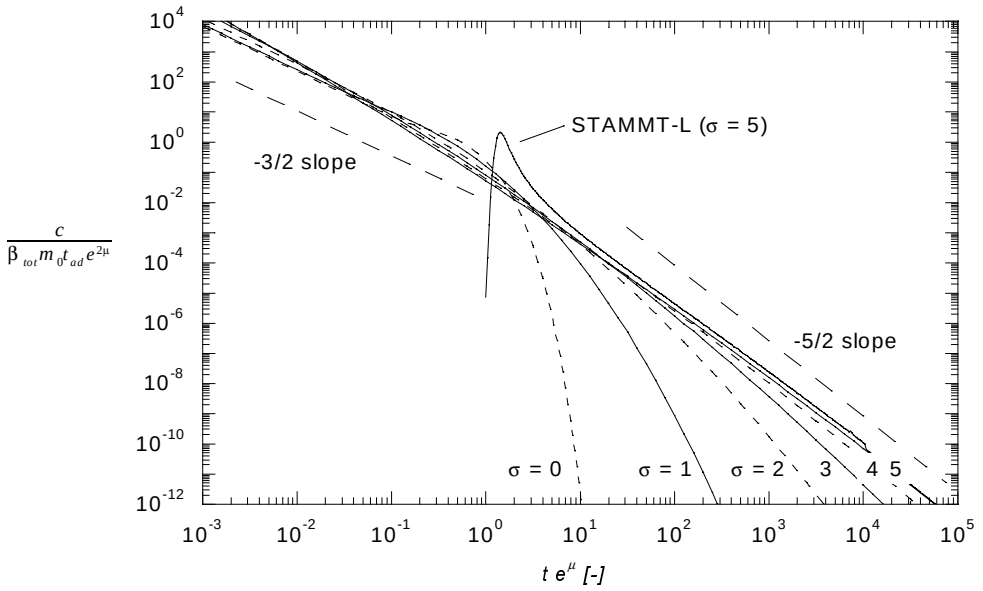

Figure 6-3. *Late-time solution and full ADMT solution for a lognormal distribution of diffusion rate coefficients.*

Published values of σ for lognormal distributions of rate coefficients are typically larger than 3 /e.g., Pedit and Miller, 1994, 1995; Culver et al, 1997; Haggerty and Gorelick, 1998/, suggesting that mass transfer rate coefficients have large variability in natural media. With such large values of σ, we would expect to see late-time slopes on double-log BTCs after a pulse-injection between 2 and 3.

6.2.4 Power law distribution of first-order rate coefficients

An alternative distribution that has been less commonly used to describe mass transfer in groundwater and soils is a power-law distribution. Hatano and Hatano /1998/ used a power-law distribution of waiting times in the context of a continuous-time random walk to model the sorption of radionuclides in a column experiment. Power-law distributions of waiting times have frequently been used in statistical physics to describe anomalous transport behavior /e.g., Bouchaud and Georges, 1990; Scher et al, 1991/. Frequently such distributions arise from diffusion or rate-limited sorption on a fractal geometry. As with a gamma distribution it is possible to define both a distribution of first-order rate coefficients and an equivalent distribution of diffusion rate coefficients. Again, although the early time behavior will differ for power-law distributions of first-order and diffusion rate coefficients, the late-time slope will be identical for the same value of *k*. For the sake of brevity, we show only the power-law distribution of first-order rate coefficients.

A general power-law distribution may be written as follows:

$$b(\alpha) = \frac{\beta_{tot}(k-2)}{\alpha_{\max}^{k-2} - \alpha_{\min}^{k-2}} \alpha^{k-3}, \quad k > 0 \; and \; k \neq 2 \tag{6-29}$$

where α_{max} [T^{-1}] is the maximum rate coefficient; α_{min} [T^{-1}] is the minimum rate coefficient; and *k* is the exponent. The value of α_{min} may be zero if $k > 2$. The reason for choosing to write the power-law as *k*-3 will become apparent shortly. If $k = 2$, the distribution may be written

$$b(\alpha) = \frac{\beta_{tot}}{\ln\left(\frac{\alpha_{max}}{\alpha_{min}}\right)}\alpha^{-1} \tag{6-30}$$

The late-time concentration in the mobile zone is

$$c = \frac{m_0 t_{ad} \beta_{tot}(k-2)}{\left(\alpha_{max}^{k-2} - \alpha_{min}^{k-2}\right)} \int_{\alpha_{min}}^{\alpha_{min}} \alpha^{k-1} e^{-\alpha t} d\alpha \,, \quad k > 0 \; and \; k \neq 2 \tag{6-31}$$

For arbitrary (non-integer) values of *k*, (6-31) must in general be evaluated numerically. However, the most important point about (6-26) is that

$$c \sim t^{-k} \,, \quad \alpha_{max}^{-1} << t << \alpha_{min}^{-1} \tag{6-32}$$

Expressed in words, the double-log slope of the BTC is -*k* for times much greater than α_{max}^{-1} and much less α_{min}^{-1} for all values of *k*. After α_{min}^{-1} the slope goes to -∞.

It is possible to present closed form solutions for many specific cases of (6-26); we will provide the solutions for the cases $k = 1$, $k = 2$, and $k = 3$. First, let us define two other variables in terms of α_{max} and α_{min}:

$$\tau = \alpha \quad t \tag{6-33}$$

$$\lambda_t = \frac{\alpha_{max}}{\alpha_{min}} \tag{6-34}$$

$$\alpha_p^2 = \begin{cases} \dfrac{\alpha_{max}^2}{1 - \lambda_t^{2-k}} \,, & k \neq 2 \\ \dfrac{\alpha_{max}^2}{\ln(\lambda_t)} \,, & k = 2 \end{cases} \tag{6-35}$$

Note that as $k \to 2$, $\alpha_p^2 \to \alpha_{max}^2 / \ln(\lambda_t)$, allowing us to use (6-35) for all values of *k*. Also note that α_p is a function of α_{max}, α_{min}, and *k*, and is used for the purpose of simplifying the following equations only.

Using these variables, the late-time concentration for $k = 1$ is therefore

$$c = m_0 t_{ad} \beta_{tot} \alpha_p^2 \left(e^{-\tau/\lambda_t} - e^{-\tau} \right) \tau^{-1} \tag{6-36}$$

If $k = 2$, then the distribution is log-uniform, and the late-time concentration is

$$c = m_0 t_{ad} \beta_{tot} \alpha_p^2 \left[e^{-\tau/\lambda_t} \left(\frac{\tau}{\lambda_t} + 1 \right) - e^{-\tau} \left(\frac{\tau}{\lambda_t} + 1 \right) \right] \tau^{-2} \tag{6-37}$$

If $k = 3$, then the distribution is uniform, and the late-time concentration is

$$c = m_0 t_{ad} \beta_{tot} \alpha_p^2 \left[e^{-\tau/\lambda_t} \left(\frac{\tau^2}{\lambda_t^2} + \frac{2\tau}{\lambda_t} + 2 \right) - e^{-\tau} \left(\tau^2 + 2\tau + 2 \right) \right] \tau^{-3} \tag{6-38}$$

From the above equations we see that a family of curves is required for each value of k since both α_{min} and α_{max} appear in all equations. However, inspection of the equations indicates that the curves for each value of k will be identical until t approaches α_{min}^{-1}.

The harmonic mean of the distribution is undefined if $k \leq 3$. Therefore, if a BTC has a late-time slope of $k \leq 3$, and the behavior is due to mass transfer, this indicates an infinite mean residence time in the immobile zone. It also causes the second and higher temporal moments of the BTC to be infinite. Note that there is nothing that physically prevents a $2 \leq k \leq 3$ as $t \rightarrow \infty$. A slope of $k \leq 2$, however, would require an infinitely large immobile zone and can therefore not be maintained for infinite time (for this reason, $k = 3/2$ is possible with diffusion, but only until $\sim a^2/D_a$). If $k > 3$ then the mean residence time would be α_{max} $(k\text{-}3)/(k\text{-}2)$, where α_{max} is the maximum rate coefficient in the distribution.

The late-time behavior of concentration, as given by (6-36) – (6-38) is shown in Figure 6-4 for $\alpha_{min} < 10^{-5}\ \alpha_{max}$. Figure 6-4 also shows the solution to the ADMT equations in the presence of a power-law distribution of rate coefficients. The ADMT equations were solved using STAMMT-L /Haggerty and Reeves, 1999/ for $m_o = 1$ s kg m^{-3}; $t_{ad} = 1$ s; $\alpha_{max} = 1$ s^{-1}; $\alpha_{min} = 1 \times 10^{-5}$ s^{-1}; $k = 1$; $\beta_{tot} = 1$; and a Peclet number of 1000.

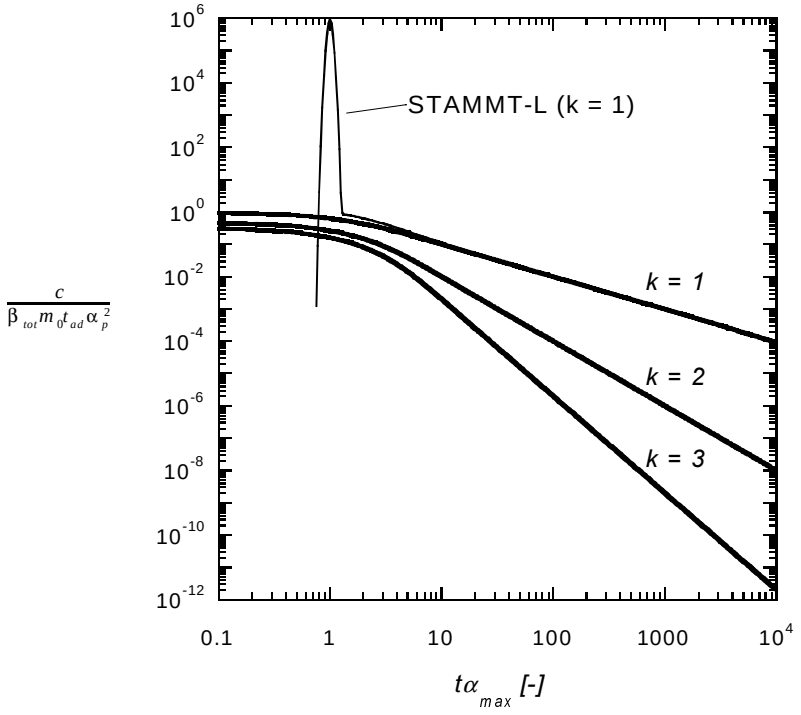

Figure 6-4. *Late-time solution and full ADMT solution for power-law distribution of first-order rate coefficients.*

6.2.5 Summary of late-time slopes

Figure 6-5 provides a summary of late-time slopes for several of the models presented. Late-time slopes are given versus nondimensional time. Note that a BTC with advection and dispersion will mask some portion of the slopes shown in this figure at earlier times. The slopes given in Figure 6-5 will only be present when $t >> t_{ad}$. A power-law slope is a constant at late-time, such as provided by the gamma and power-law distributions. Note that conventional diffusion model is equivalent to the lognormal distribution with $\sigma = 0$. The slope in the conventional model is –3/2 until approximately the mean residence time in the immobile zone ($a^2/3D_a$ for 1-D diffusion). Note that the lognormal distribution with larger s cannot provide a true power-law BTC, but can hold the slope relatively constant over a long time. All lognormal distributions will reach an infinite slope at infinite time.

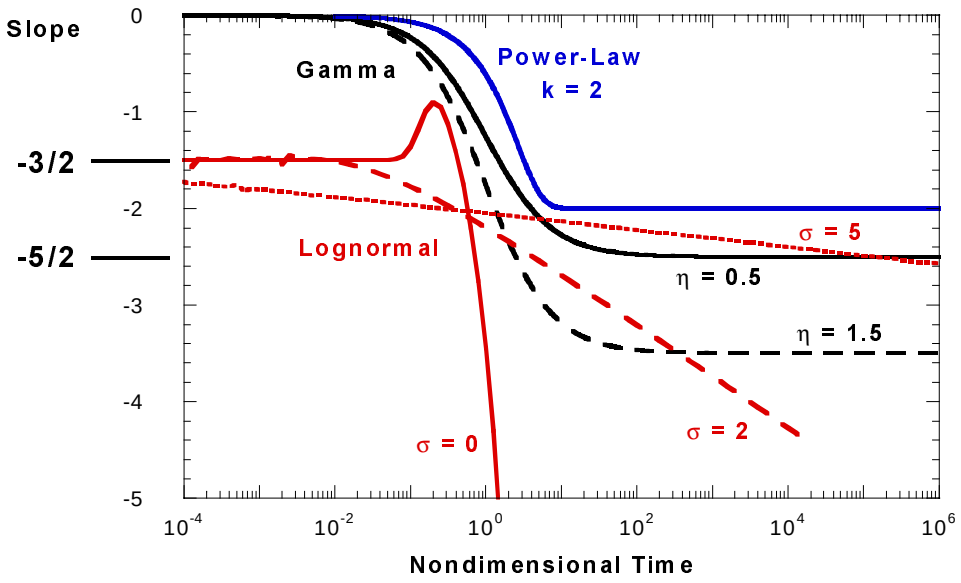

Figure 6-5. *Slopes of late-time double-log breakthrough curves. Note that while the breakthrough curve is dominated by advection and dispersion, the slopes will be different from that shown here.*

6.3 Discussion and implications

6.3.1 Particular considerations with power-law BTC behavior

We note again that both the gamma and power-law distributions behave as power-laws for small α or D_a/a^2, and result in predicted power-law BTCs at late time. The conventional diffusion model also causes power-law BTCs prior to $t \sim a^2/D_a$. There are four important possibilities of such power-law behavior.

CASE 1 – Power-law behavior to infinite time and k < 3: The first possibility is that the BTC behaves as a power law over all time (i.e., the slope of the BTC would be power-law to infinite time) and the slope is less than 3. It is important to note that this is physically possible provided that the slope *k* is greater than 2. In Case 1, the mean residence time in the immobile zone must be infinite. Consequently, there can be no effective single-rate model that is equivalent to the multirate model in the way that a single-rate first-order model is equivalent to a conventional single-rate diffusion model. No single-rate (either first-order or diffusion) model can yield the same second or higher temporal moments as the multirate model. Any single-rate model (either first-order or diffusion) will have parameters that are a function of the experimental observation time (i.e., the experiment length).

CASE 2 – Power-law behavior longer than experimental time-scale and k < 3: The second possibility is that the power-law behavior ends at a particular time but beyond the experimental observation time, and the slope is less than 3. In this case, the mean residence time in the immobile zone cannot be ascertained from the experimental data alone. In other words, it is not possible, based solely on the BTC data, to estimate an effective rate coefficient: the effective rate coefficient could be non-existent (as in the power-law behavior to infinity case) or simply longer than the inverse of the experimental time. An important point is that if the slope *k* is less than 2, then the power-law

behavior either must end at some time or the slope must steepen to greater than 2. Such is the case with conventional diffusion and a slope of –3/2. Because the immobile zone cannot be infinitely thick, the power-law behavior must end at some time. However, without information external to the tracer test data, the time at which the power-law behavior ends (and therefore the mean residence time in the immobile zone) cannot be known.

CASE 3 – Power-law behavior ends within experimental time-scale: The third possibility is that the power-law behavior ends within the experimental observation time. This is the case of the conventional diffusion model with an intermediate slope of –3/2. In this case, then an effective rate coefficient or mean residence time in the immobile zone can be estimated, and will be approximately the inverse of the time at which the power-law behavior ends. Note that Case 3 cannot be modeled by a gamma distribution because a gamma distribution does not allow for an end to the power-law behavior.

CASE 4 – Power-law behavior with k > 3: The fourth possibility is that the BTC has a slope less than 3. In this case the mean residence time can be estimated even if the power-law behavior extends to infinite time. This is because the harmonic mean of a power-law distribution is non-zero provided that $k \leq 3$.

6.4 Late-time slope conclusions

With improvements in experimental and analytical techniques, concentrations are now available from many laboratory and field experiments over several decades of both time and concentration. The late-time behavior of breakthrough curves (BTCs) is critically important to the evaluation of rate-limited mass transfer, especially if discrimination between different models of mass transfer is desired. Double-log plots of BTCs are particularly helpful and commonly can be used to distinguish between the effects of dispersion and the effects of mass transfer. We have six primary conclusions.

First, we derived a simple analytical expression for late-time BTC behavior in the presence of mass transfer. Equation (6-14) gives the late-time concentration for any linear rate-limited mass transfer model for either zero-concentration or equilibrium initial conditions. The expression requires that advection time-scale, the zeroth moment of the injection pulse, the initial concentration in the system, and the memory function $g(t)$.

Second, the memory function $g(t)$ is proportional to the residence time distribution in the immobile zone given a unit impulse at the surface of the immobile zone. This memory function is simply the derivative of the Laplace transform of the distribution of rate coefficients describing the immobile zone. Consequently, the late-time concentration is proportional to the first or second derivative of the Laplace transform of the distribution of rate coefficients.

Third, the effective rate coefficient that yields the same zeroth, first, and second temporal moments in the BTC is the harmonic mean of the distribution of rate coefficients. However, for any distribution of rate coefficients with power-law $\alpha^{\eta-1}$ and where $\eta<1$, the harmonic mean is zero. Consequently the mean residence time in the immobile zone is infinite and there is no effective rate coefficient. This applies both to distributions of diffusion rate coefficients and distributions of first-order rate coefficients.

Fourth, if the a BTC (after a pulse injection) goes as $\sim t^{-k}$ as $t \rightarrow \infty$, then the underlying distribution of rate coefficients must be $\sim \alpha^{k-3}$ as $\alpha \rightarrow 0$. This holds for either distributions of first-order and diffusion rate coefficients. For a BTC from a medium with initially non-zero but equilibrium concentrations, then the equivalent BTC goes as t^{-k+1}.

Fifth, if the slope of a BTC (after a pulse injection) goes as $\sim t^{-k}$ as $t \rightarrow \infty$, and $k \leq 3$, then the mean residence time in the immobile zone is infinite. (This is a corollary to the third and fourth conclusions.) Consequently there is no effective rate coefficient in this medium. A second consequence is that any single-rate (either diffusion or first-order) rate coefficient estimated from the BTC will be a function of experimental observation time. Again, for a BTC from a medium with initially non-zero but equilibrium concentrations, then the equivalent BTC goes as t^{-k+1}.

Sixth, if a BTC exhibits power-law behavior ($c \sim t^{-k}$) to the end of the experiment, then one of two cases must exist. If $k \leq 3$ then the mean residence time (and effective rate coefficient) cannot be estimated from the BTC. The mean residence time must be at least the experimental observation time and could be infinite. If $k > 3$ then the mean residence time (and its inverse the effective rate coefficient) can be estimated. For example, in the case of a power-law distribution, the effective rate coefficient would be α_{max} $(k\text{-}3)/(k\text{-}2)$, where α_{max} is the maximum rate coefficient in the distribution.

7 Consequences of multirate and anomalous diffusion for nuclear waste disposal

The consequences of multirate and anomalous diffusion for nuclear waste disposal were discussed in Section 2; however, it is worth emphasizing them. If anomalous diffusion occurs within rock, the most important physical and modeling consequences for nuclear waste disposal are summarized as below.

1. No single value of diffusivity can represent the diffusion process at all time- or length-scales. Expressed in another manner, any single diffusivity is representative of diffusion only at one time- or length-scale.

2. The diffusivity decreases with both time- and length-scale of measurement. The mean diffusivity for true anomalous diffusion approaches zero at very large time- or length-scales (i.e., the pore space at very large distances is very poorly connected).

3. The porosity of the matrix may not be entirely accessed by a solute diffusing through the pores. Some fraction of the porosity may remain inaccessible via aqueous diffusion for all time.

4. Given a model of diffusion using a single diffusivity, some fraction of the porosity will be accessed less quickly than a Fickian model of diffusion would predict.

5. Laboratory measurements using the through-diffusion approach (e.g., Skagius and Neretnieks, 1986) will yield diffusivities that decrease with sample length.

6. Laboratory measurements that allow diffusion in and out of the same surface and that depend on the tail concentration for an estimate of diffusivity (e.g., column experiments, purge experiments, batch ,“desorption” experiments) will yield diffusivities that decrease with experimental time (assuming a single diffusivity is estimated).

7. A transport model incorporating advection and matrix diffusion and that assumes the total matrix porosity is accessible by diffusion will over-estimate the late-time retardation of the solute plume. Performance Assessment transport calculations would therefore be non-conservative.

The consequences of multirate diffusion are identical to those of anomalous diffusion (since the concept of multirate diffusion can include anomalous diffusion), but with the following exceptions.

1. Through-diffusion measurements may not yield diffusivities that decrease with sample length. This is because pores and pore networks with different diffusivities may each span the length of all samples. In this case, the estimated diffusivity will tend to be dominated by the largest values of diffusivity (see Footnote 4, page 16, for more detail).

2. Multirate diffusion would not necessarily prevent diffusion from accessing all pore space. However, it is still true that given a model of diffusion using a single

diffusivity, some fraction of the porosity will be accessed less quickly than a single-rate model of diffusion would predict.

3. Over some range of times, no single value of diffusivity can represent the diffusion process. However, provided that the distribution of D_d/a^2 has a non-zero harmonic mean, then a single value of diffusivity can represent the diffusion process at long enough time (see Section 6.3.1).

8 References

Acuna J A, Yortsos Y C, 1995. Application of fractal geometry to the study of networks of fractures and their pressure transient. Water Resour. Res., 31(3), 527–540.

Aharonov E, Rothman D H, Thompson A H, 1997. Transport properties and diagenesis in sedimentary rocks: The role of micro-scale geometry. Geology, 25(6), 547–550.

Alberty W J, Bartlett P N, Wilde C P, Darwent J R, 1985. A general model for dispersed kinetics in heterogeneous systems. J. Am. Chem. Soc., 107(7), 1854–1858.

Avnir D, Farin D, Pfeifer P, 1984. Molecular fractal surfaces. Nature, 308, 261–263.

Backes E A, McLaren R G, Rate A W, Swift R S, 1995. Kinetics of cadmium and cobalt desorption from iron and manganese oxides. Soil Sci. Soc. Am. J., 59(3), 778–785.

Ball W P, Roberts P V, 1991. Long-term sorption of halogenated organic-chemicals by aquifer material, 2, Intraparticle diffusion. Environ. Sci. Technol., 25(7), 1237–1249.

Birgersson L, Neretnieks I, 1982. Diffusion in the matrix of granitic rock, Field test in the Stripa mine, Scientific Basis for radioactive Waste Management – V. Elsevier, 519–528.

Birgersson L, Neretnieks I, 1984. Diffusion in the matrix of granitic rock, Field test in the Stripa mine, Part 2. Mat. Res. Soc. Symp. Proc. 26, 247–254.

Birgersson L, Neretnieks I, 1990. Diffusion in the matrix of granitic rock: Field test in the Stripa mine. Water Resour. Res., 26(11), 2833–2842.

Bouchaud J-P, Georges A, 1990. Anomalous diffusion in disordered media: Statistical mechanisms, models and physical applications. Phys. Rep., 195(4 & 5), 127–293.

Brusseau M L, 1992. Nonequilibrium transport of organic chemicals: The impact of pore-water velocity. J. Contam. Hydrol., 9, 353–368.

Byegård J, Albinsson Y, Skarnemark G, Skålberg M, 1992. Field and Laboratory studies of the reduction and sorption of technetium. Radiochim. Acta, 58/59, 239–244.

Byegård J, Johansson H, Skålberg M, Tullborg E-L, 1998. The interaction of sorbing and non-sorbing tracers with different Äspö rock types: Sorption and diffusion experiments in the laboratory scale. SKB TR-98-18, Swedish Nuclear Fuel and Waste Management Co.

Byegård J, Andersson P, Johansson H, Hansson K, Winberg A, 1999. Äspö Hard Rock Laboratory Test Plan for the Long-Term Diffusion. Release 1.2, Incomplete first draft, February 22.

Carrera J, Sánchez-Vila X, Benet I, Medina A, Galarza G, Guimerà J, 1998. On matrix diffusion: Formulations, solution methods and qualitative effects. Hydrogeology Journal, 6, 178–190.

Chen W, Wagenet R J, 1995. Solute transport in porous media with sorption-site heterogeneity. Environ. Sci. Technol., 29, 2725–2734.

Chen W, Wagenet R J, 1997. Description of atrazine transport in soil with heterogeneous nonequilibrium sorption. Soil Sci. Soc. Am. J., 61(2), 360–371.

Connaughton D F, Stedinger J R, Lion L W, Shuler M L, 1993. Description of time-varying desorption kinetics: Release of naphthalene from contaminated soils. Environ. Sci. Technol., 27(12), 2397–2403.

Cooney D O, Adesanya B A, Hines A L, 1983. Effect of particle size distribution on adsorption kinetics in stirred batch systems. Chem. Eng. Sci., 38, 1535–1541.

Crank J, 1975. The Mathematics of Diffusion. 2nd ed. Oxford Univ. Press, New York.

Culver T B, Hallisey S P, Sahoo D, Deitsch J J, Smith J A, 1997. Modeling the desorption of organic contaminants from long-term contaminated soil using distributed mass transfer rates. Environ. Sci. Technol., 31(6), 1581–1588.

Cunningham J A, Werth C J, Reinhard M, Roberts P V, 1997. Effects of grain-scale mass transfer on the transport of volatile organics through sediments, 1, Model development. Water Resour. Res., 33(12), 2713–2726.

Cunningham J A, Roberts P V, 1998. Use of temporal moments to investigate the effects of nonuniform grain-size distribution on the transport of sorbing solutes. Water Resour. Res., 34(6), 1415–1425.

Delascuevas C, 1997. Pore structure characterization in rock-salt. Eng. Geol., 47(1–2), 17–30.

Eikenberg J, Hoehn E, Fierz Th, Frick U, 1994. Grimsel Test Site: Preparation and performance of migration experiments with radioisotopes of sodium, strontium and iodine. Paul Scherrer Inst., Würenlingen, PSI-Bericht No. 94-11.

Farrell J, Reinhard M, 1994. Desorption of halogenated organics from model solids, sediments, and soil under unsaturated conditions. 2., Kinetics, Environ. Sci. Technol., 28(1), 63–72.

Fong F K, Mulkey L A, 1990. Solute transport in aggregated media: Aggregated size distribution and mean radii. Water Resour. Res., 26(6), 1291–1303.

Gelhar L W, 1993. Stochastic Subsurface Hydrology. Prentice-Hall, Englewood Cliffs, USA.

Gelhar L W, Welty C, Rehfeldt K R, 1992. A critical review of data on field-scale dispersion in aquifers. Water Resour. Res., 28(7), 1955–1974.

Giona M, Schwalm W A, Schwalm M K, Adrover A, 1996a. Chem. Eng. Sci., 51(20), 4717–4729.

Giona M, Schwalm W A, Schwalm M K, Adrover A, 1996b. Exact solution of linear transport equations in fractal media – II. Diffusion and convection. Chemical Engineering Science, 51(20), 4731–4744.

Glueckauf E, 1955. Part 10., Formulae for diffusion into spheres and their application to chromatography. Transactions of the Faraday Society, 51, 1540–1551.

Goltz M N, Roberts P V, 1986. Interpreting organic solute transport data from a field experiment using physical nonequilibrium models. J. Contam. Hydrol., 1(1), 77–93.

Goltz M N, Roberts P V, 1987. Using the method of moments to analyze three-dimensional diffusion-limited solute transport from temporal and spatial perspectives. Water Resour. Res., 23(8), 1575–1585.

Ghosh A, Daemen J J K, 1993. Fractal characteristics of rock discontinuities. Eng. Geol., 34(1–2), 1–9.

Grathwohl P, Pyka W, Merkel P, 1994. Desorption of organic pollutants (PAHs) from contaminated aquifer materials. Transport and Reactive Processes in Aquifers. Edited by T H Dracos and F Stauffer, Balkema, Rotterdam, 469–474.

Griffioen J W, Barry D A, Bajracharya K, 1997. Comment on “Effect of solute size on transport in structured porous media” by Qinhong Hu and Mark L. Brusseau. Water Resour. Res., 33(2), 359–361.

Griffioen J W, Barry D A, Parlange J-Y, 1998. Interpretation of two-region model parameters. Water Resour. Res., 34(3), 373–384.

Hadermann J, Heer W, 1996. The Grimsel (Switzerland) migration experiment: Integrating field experiments, laboratory investigations and modelling. J. Contam. Hydrol., 21, 87–100.

Haggerty R, 1995. Aquifer Remediation in the Presence of Rate-Limited Mass Transfer, PhD Dissertation. Stanford University, Stanford, Calif.

Haggerty R, Gorelick S M, 1995. Multiple-rate mass transfer for modeling diffusion and surface reactions in media with pore-scale heterogeneity. Water Resour. Res., 31(10), 2383–2400.

Haggerty R, Harvey C F, 1997. A comparison of estimated mass transfer rate coefficients with the time-scales of the experiments from which they were determined. Eos, 78(46), F293.

Haggerty R S, Fleming S W, Meigs L C, McKenna S A, 1998. Tracer tests in a fractured dolomite 3. Analysis of mass transfer in single-well injection-withdrawal tests, submitted to Water Resour. Res., December.

Haggerty R, Gorelick S M, 1998. Modeling mass transfer processes in soil columns with pore-scale heterogeneity. Soil Sci. Soc. Am. J., 62(1), 62–74.

Haggerty R, Reeves P, 1999. STAMMT-L: Solute Transport and Multirate Mass Transfer, User's manual. Sandia National Laboratories, Albuquerque, NM.

Hartikainen J, Hartikainen K, Hautojärvi A, Kuoppamäki K, Timonen J, 1996. Helium gas method for rock characteristics and matrix diffusion. Posiva-96-22, Posiva Oy, Helsinki, Finland.

Hatano Y, Hatano N, 1998. Dispersive transport of ions in column experiments: An explanation of long-tailed profiles. Water Resour. Res., 34(5), 1027–1033.

Havlin S, Ben-Avraham D, 1987. Diffusion in disordered media. Adv. Phys., 36(6), 695–798.

Hollewand M P, Gladden L F, 1995. Transport heterogeneity in porous pellets – 2., NMR imaging studies under transient and steady-state conditions. Chem. Eng. Sci., 50(2), 327–344.

Hu X J, Do D D, 1994. Effect of surface heterogeneity on the adsorption-kinetics of gases in activated carbon: Pore-size distribution vs. energy-distribution. Langmuir, 10(9), 3296–3302.

Hughes B D, 1994. Random Walks, Percolation, and Fractals. Oxford University Press.

Ittner T, Torstenfelt B, Allard B, 1990. Diffusion of strontium, technetium, iodine and cesium in granitic rock. Radiochimica Acta, 49, 101–106.

Johansson H, Byegård J, Skarnemark G, Skålberg M, 1997. Matrix diffusion of some alkali- and alkaline earth metals in granitic rock. Mat. Res. Soc. Symp. Proc., 465, 871–878.

Johansson M, Siitari-Kauppi, Skålberg M, Tullborg E-L, 1998. Diffusion pathways in crystalline rock – examples from Äspö diorite and fine-grained granite. J. Contam. Hydrol., 35(1-3), 41–53.

Katz A J, Thompson A H, 1985. Fractal sandstone pores: Implications for conductivity and pore formation. Phys. Rev. Let., 54(12), 1325–1328.

Krohn C, 1988. Sandstone fractal and Euclidian pore volume distributions. J. Geophys. Res., 93(B4), 3286–3296.

Lafolie F, Hayot Ch, 1993. One-dimensional solute transport modelling in aggregated porous media, Part 1, Model description and numerical solution. J. Hydrol., 143, 63–83.

Li L, Barry D A, Culligan-Hensley P J, Bajracharya K, 1994. Mass transfer in soils with local stratification of hydraulic conductivity. Water Resour. Res., 30(11), 2891–2900.

Lorden S W, Chen W, Lion L W, 1998. Experiments and modeling of the transport of trichloroethene vapor in unsaturated aquifer material, Environ. Sci. Technol., 32(13), 2009–2017.

Lovera O M, Richter F M, Harrison T M, 1989. The $^{40}Ar/^{39}Ar$ thermochronometry for slowly cooled samples having a distribution of diffusion domain sizes. J. Geophys. Res., 94, 17917–17935.

McKenna S A, Meigs L C, Haggerty R, 1998. Tracer tests in a fractured dolomite, 4. Double-porosity, multiple-rate mass transfer processes in two-well convergent flow tests, submitted to Water Resour. Res., December. In revision.

Meigs L C, Beauheim R L. Tracer tests in a fractured dolomite, 1. Experimental design and observed tracer recoveries. Water Resour. Res., in review.

Muralidhar R, Ramkrishna D, 1993. Diffusion in pore fractals: A review of linear response models. Transp. Por. Media, 13, 79–95.

National Research Council, 1996. Rock Fractures and Fluid Flow. National Academy Press.

Neretnieks I, 1993. Solute transport in fractured rock – Applications to radionuclide waste repositories, in Flow and Contaminant Transport in Fractured Rock, edited by J Bear, C-F Tsant, and G de Marsily. Academic Press, New York, 39–127.

Neretnieks I, 1980. Diffusion in the rock matrix: An important factor in radionuclide transport?. J. Geophys. Res., 85(B8), 4379–4397.

Neretnieks I, Rasumuson A, 1984. An approach to modelling radionuclide migration in a medium with strongly varying velocity and block sizes along the flow path. Water Resour. Res., 20(12), 1823–1836.

Ohlsson Y, Neretnieks I, 1995. Literature survey of matrix diffusion theory and of experiments and data including natural analogues. SKB TR 95-12, Swedish Nuclear Fuel and Waste Management Co.

Ohlsson Y, Neretnieks I, 1997. Diffusion data in granite – Recommended values. SKB TR 97-20, Swedish Nuclear Fuel and Waste Management Co.

Pedit J A, Miller C T, 1994. Heterogeneous sorption processes in subsurface systems, 1., Model formulations and applications. Environ. Sci. Technol., 28(12), 2094–2104.

Pedit J A, Miller C T, 1995. Heterogeneous sorption processes in subsurface systems, 2, Diffusion modeling approaches. Environ. Sci. Technol., 29(7), 1766–1772.

Rao P S C, Jessup R E, Addiscott T M, 1982. Experimental and theoretical aspects of solute diffusion in spherical and nonspherical aggregates. Soil Science, 133(6), 342–349.

Rasmuson A, 1985. The effect of particles of variable size, shape and properties on the dynamics of fixed beds. Chem. Eng. Sci., 40(4), 621–629.

Rasmuson A, 1986. Modeling of solute transport in aggregated/fractured media including diffusion into the bulk matrix. Geoderma, 38, 41–60.

Rate A W, McLaren R G, Swift R S, 1992. Evaluation of a log-normal distribution 1st-order kinetic model for copper(II)-humic acid complex dissociation. Environ. Sci. Technol., 26(12), 2477–2483.

Roberts G E, Kaufman H, 1966. Table of Laplace Transforms. W B Saunders Co., Philadelphia.

Ruthven D M, Loughlin K F, 1971. The effect of crystallite shape and size distribution on diffusion measurements in molecular sieves. Chem. Eng. Sci., 26, 577–594.

Sahimi M, 1993. Fractal and superdiffusive transport and hydrodynamic dispersion in heterogeneous porous media. Transp. Por. Med., 13, 3–40.

Sahimi M, 1995. Flow and Transport in Porous Media and Fractured Rock: From Classical Methods to Modern Approaches. VCH, New York.

Satterfield C N, Colton C K, Pitcher W H Jr., 1973. Restricted diffusion in liquids within fine pores. AIChE J., 19(3), 628–635.

Scher H, Shlesinger M F, Bendler J T, 1991. Time-scale invariance in transport and relaxation. Physics Today, January, 26-34.

Schirmacher W, 1991. Anomalous diffusion in disordered systems: An effective medium description, Ber. Bunsenges. Phys. Chem., 95(3), 368–376.

Schwalm W A, Schwalm M K, 1988. Extension theory for lattice Green functions. Phys. Rev. B., 37(16), 9524–9542.

Sheintuch M, Brandon S, 1989. Deterministic approaches to problems of diffusion, reaction and adsorption in a fractal porous catalyst. Chemical Eng. Sci., 44(1), 69ff.

Skagius K, Neretnieks I, 1986. Diffusion in crystalline rocks of some sorbing and non-sorbing species. In: K Skagius PhD Dissertation, KTH, Stockholm.

Sworakowski J, Nespurek S, 1998. A straightforward method of analysis of first-order processes with distributed parameters. Chem. Phys. Lett., 298(1–3), 21–26.

Thompson A H, Katz A J, Krohn C E, 1987. The microgeometry and transport properties of sedimentary rock, Advances in Physics, 36, 625–694.

Tsukamoto M, Ohe T, 1993. Effects of biotite distribution on cesium diffusion in granite. Chem. Geol., 107, 29–46.

Turcotte D L, 1986. Fractals and fragmentation. J. Geophys. Res., 91(B2), 1921–1926.

Valkiainen M, 1992. Diffusion in the rock matrix – A review of laboratory tests and field studies, Report YJT-92-04. Nuclear Waste Commission of Finnish Power Companies, Helsinki.

Valkiainen M, Aalto H, Lehikoinen J, Uusheimo K, 1996. The effect of thickness in the through-diffusion experiment, Final report. VTT Research Notes 1788, Technical Research Centre of Finland, Espoo.

Valocchi A J, 1990. Use of temporal moment analysis to study reactive solute transport in aggregated porous media. Geoderma, 46, 233–247.

van Genuchten M, Th, Tang D H, Guennelon R, 1984. Some exact solutions for solute transport through soils containing large cylindrical macropores. Water Resour. Res., 20(3), 335–346.

Villermaux J, 1981. Theory of linear chromatography, in Percolation Processes, Theory and Applications, edited by E Rodrigues and D Tondeur, NATO ASI Series E, vol. 33. Sijthoff and Noordhoff, Rockville, Mass., 83–140.

Wadden M M, Katsube T J, 1982. Radionuclide diffusion rates in igneous crystalline rocks. Chem. Geol., 36, 191–214.

Wang K, Do D D, 1999. Sorption equilibria and kinetics of hydrocarbons onto activated carbon samples having different micropore size distributions. Adsorption – Journal of the International Adsorption Society, 5(1), 25–37.

Werth C J, Cunningham J A, Roberts P V, Reinhard M, 1997. Effects of grain-scale mass transfer on the transport of volatile organics through sediments, 2, Column results. Water Resour. Res., 33(12), 2727–2740.

Winberg A, 1999. Technical memorandum: Continued strategy for TRUE-2 and LTDE, included as Appendix 5 of O Olsson, Minutes of Review Meeting for TRUE and Long-Term Diffusion Experiment (LTDE), May 14.

Xu S, Worman A, 1997. An investigation of heterogeneity of porosity and diffusivity in crystalline rock. Eos, 78(46), 330–331.

Young D F, Ball W P, 1995. Effects of column conditions on the first-order rate modeling of nonequilibrium solute breakthrough. Water Resour. Res., 31(9), 2181–2192.

9 Appendix: Definitions of variables

a	size of immobile zone; half-block size [L]
a_w	specific surface area of a fracture [L^{-1}]
$b(\alpha)$	density function of rate coefficients; see Eqn. (6-16) and Table 6-1.
c	concentration in mobile zone (pores, well, etc.) [M/L^3]
c_b	injection concentration in immobile zone [M/L^3]
c_m	concentration in the immobile zone (rock matrix) [M/L^3]
c_{obs}	concentration in the observation well [M/L^3]
c_0	initial concentration [M/L^3]
c_1	concentration one node inside fractal lattice [M/L^3]
D	aqueous diffusivity [L^2/T]
D_a	apparent diffusivity (equal to pore diffusivity divided by retardation factor for rock matrix) [L^2/T]
D_p	pore diffusivity [L^2/T]
D_L	dispersion coefficient in transport direction [L^2/T]
d_s	spectral dimension [-]
d_w	walk dimension [-]
$\boldsymbol{e_1}$	vector $(1,0,\ldots,0)^T$ where T indicates transpose
$f(*)$	a density function
$\boldsymbol{G}(z)$	Green function; see Eqn. (5-3) and (5-4)
$g(t)$	memory function; see discussion after Eqn. (6-10) and Table 6-1.
H_{ij}	adjacency matrix (discrete notation)
$\boldsymbol{H}$	adjacency matrix (matrix notation)
$\boldsymbol{I}$	identity matrix
$I_0(\omega)$	Bessel function
$I_1(\omega)$	Bessel function

i	imaginary number
K_d	distribution coefficient [L^3/M]
K_a	surface equilibrium constant [L]
$K_0(\omega)$	Bessel function
$K_1(\omega)$	Bessel function
k	slope of a breakthrough curve on a double-logarithmic plot
L	length of system [L]
$Lap\{*\}$	Laplace transform
$M(\omega)$	see Eqn. (4-18)
m_0	zeroth moment of the concentration history [MT/L^3]
$N(\omega)$	see Eqn. (4-19)
P	Peclet number; see Eqn. (4-12) [-]
p	coordination number on fractal lattice
Q	pumping rate [L^3/T]
Q^*	flushing rate [1/T]
$R(t)$	radius of displacement of a molecule from its origin over time [L]
R_a	retardation factor due to surface sorption in mobile zone [-]
R_i	radius of the injection well [L]
R_{im}	retardation factor specifically for immobile zone (matrix rock) [-]
R_m	retardation factor for mobile zone (could be equivalent to R_a) [-]
R_o	distance from the center of the injection well to the edge of the matrix [L]
R_w	distance from the center of the injection well to the observation well [L]
r	radial coordinate [L]
r_{obs}	radius of the observation well [L]
s	Laplace parameter [T^{-1}]
t	time [T]
t_{ad}	advection time; see discussion after Eqn. (6-5)

t_α mass transfer time [T^{-1}]

u_j root of a Bessel function equation; see Table 6-1.

V sparse matrix; see Eqn. (5-4)

v velocity in transport direction

x coordinate [L]

Z nondimensional coordinate; see Eqn. (4-11) [-]

z coordinate [L]; modified Laplace parameter in Eqn. (5-3).

α rate coefficient [T^{-1}]

α^* rate coefficient, specifically for a first-order mass transfer model [T^{-1}]

α_H harmonic mean of the rate coefficient density function $b(\alpha)$; see Table 6-1[T^{-1}]

α_L dispersivity [L]

α_{min} minimum rate coefficient in power-law distribution; see Eqn. (6-29)

α_{max} minimum rate coefficient in power-law distribution; see Eqn. (6-29)

α_p see Eqn. (6-35)

β_{tot} capacity coefficient [-]; equal to the ratio of mass in the mobile zone to mass in the immobile zone at equilibrium

$\delta(t)$ Dirac impulse [T^{-1}]

δ_D constrictivity [-]

δ_{il} Kronecker delta

Δx fractal lattice (node-node) size [L]

$\Gamma(t)$ source-sink term; see Eqn. (6-1)

γ a parameter of gamma distribution [T^{-1}]

η parameter in gamma distribution [-]

λ dimensionless diffusivity; see Eqn. (4-15) [-]

λ_t ratio of rate coefficients in power-law distribution.

μ parameter in lognormal distribution; see Eqn. (6-28)

ξ dimensionless radius; see Eqn. (4-13) [-]

ξ_o dimensionless radius at the edge of the system; see Eqn. (4-14) [-]

ϕ porosity [-]

θ_{im} porosity; specificall, the porosity of the immobile zone (matrix rock) [-]

ρ bulk density [M/L^3]

σ parameter in lognormal distribution; see Eqn. (6-28)

τ dimensionless time; see Eqn. (4-10) [-]. Also can be dummy variable of integration.

τ_t^2 tortuosity [-]

ω see Eqn. (4-17)